JAMES | Journal of Advances in Modeling Earth Systems

RESEARCH ARTICLE
10.1029/2021MS002677

Relating Vertical Velocity and Cloud/Precipitation Properties: A Numerical Cloud Ensemble Modeling Study of Tropical Convection

W.-K. Tao[1], T. Iguchi[1,2], S. Lang[1,3], X. Li[1,4,5], K. Mohr[6], T. Matsui[1,2], S. C. van den Heever[7], and S. Braun[1]

[1]Mesoscale Atmospheric Processes Laboratory, NASA Goddard Space Flight Center, Greenbelt, MD, USA, [2]Earth System Science Interdisciplinary Center, University of Maryland, College Park, MD, USA, [3]Science Systems and Applications, Inc., Lanham, MD, USA, [4]Goddard Earth Sciences Technology and Research II, Morgan State University, Baltimore, MD, USA, [5]Now at Climate Science Division, School of Computer, Mathematical, and Natural Sciences, Morgan State University, Baltimore, MD, USA, [6]Earth Sciences Division, NASA Goddard Space Flight Center, Greenbelt, MD, USA, [7]Department of Atmospheric Science, Colorado State University, Fort Collins, CO, USA

Abstract Fundamental relationships exist between cloud and precipitation development and their dynamic processes. Latent heat released by cloud/precipitation formation affects cloud vertical motions, which in turn affect convective cloud development. Here, a cloud-resolving model is used to relate cloud properties and latent heating with cloud drafts using 15-day simulations for an oceanic and continental environment. The results show condensation, deposition, and freezing occur mainly in moderate (3–5 m s^{-1}) to strong (>10 m s^{-1}) updrafts, evaporation and sublimation mainly in weak (1–2 m s^{-1}) to moderate downdrafts, and melting in moderate updrafts and downdrafts. Active updrafts cover only a small percentage of the model domain but contribute significantly to the latent heat release and are associated with large proportions of the hydrometeors. Active updrafts with vertical velocities exceeding 1 and 2 m s^{-1} account for more than 75% and 50%, respectively, of the condensation, deposition, and freezing in both the oceanic and continental cases. However, active downdrafts with vertical velocity magnitudes exceeding |1 m s^{-1}| account for less than 40% and 25%, respectively, of the evaporation and sublimation. More evaporation and sublimation than condensation and deposition occur in the inactive cloud regions. Sensitivity tests are also conducted to assess the impact of model grid spacing (1,000 m vs. 250 m) and microphysical schemes (3 ice classes vs. 4 ice classes) on latent heat release and hydrometeor amount. The results show that model resolution had more impact than the microphysics on the simulated cloud properties in both cases.

Plain Language Summary Long-term, 2D Goddard Cumulus Ensemble model simulations for one tropical oceanic (Dynamics of the Madden-Julian Oscillation) and one tropical continental (Green Ocean Amazon Experiment) case were conducted to examine the relationship between latent heating (LH) processes and cloud properties (hydrometeors) with respect to the vertical velocity. The model simulated a population of different types of clouds and convective systems over their respective life cycles in both cases. The simulated LH processes and cloud properties were then separated into convective and stratiform regions, as well as active and inactive cloud regimes. The results show that almost all condensation, deposition, and freezing occur in the upward motion region while evaporation and sublimation mainly are in the downward motion region. Melting can occur in both updraft and downdraft regions. The results also indicate that active updrafts cover only a small area (a few percent) of the model domain where the most condensation and freezing occur. But more evaporation and sublimation occur in the inactive downdraft regions. Sensitivity tests show that the model resolution (250 and 1,000 m) had more impact than the microphysical scheme (3 classes of ice vs. 4 classes ice) on the simulated cloud properties in both cases.

Key Points:

- Two-dimensional cloud-resolving model simulations show that storm dynamics and cloud microphysics are strongly coupled
- Condensation, deposition, and freezing concentrate mainly in moderate to strong updrafts, which occupy a small area of the model domain
- Evaporation and sublimation process occur in weak to moderate downdrafts over a more extensive area

Supporting Information:

Supporting Information may be found in the online version of this article.

Correspondence to:

X. Li,
Xiaowen.Li@morgan.edu

Citation:

Tao, W.-K., Iguchi, T., Lang, S., Li, X., Mohr, K., Matsui, T., et al. (2022). Relating vertical velocity and cloud/precipitation properties: A numerical cloud ensemble modeling study of tropical convection. *Journal of Advances in Modeling Earth Systems*, *14*, e2021MS002677. https://doi.org/10.1029/2021MS002677

Received 14 JUL 2021
Accepted 20 JUL 2022

Author Contributions:

Conceptualization: W.-K. Tao, K. Mohr, T. Matsui, S. C. van den Heever, S. Braun
Formal analysis: W.-K. Tao, T. Iguchi, S. Lang
Investigation: S. Lang, K. Mohr
Methodology: W.-K. Tao, T. Iguchi, S. Lang, T. Matsui, S. C. van den Heever, S. Braun

1. Introduction

Cloud-scale vertical motion and microphysical processes are related. Latent heat release (heating through condensation, deposition, and freezing) enhances upward motion while heat loss (cooling through evaporation, sublimation, and melting) enhances downward motion. The results of these microphysical processes produce or remove various types of cloud particles (hydrometeors), from small cloud droplets and ice particles to large rain drops and

Resources: K. Mohr, T. Matsui, S. C. van den Heever, S. Braun
Software: T. Iguchi, S. Lang, T. Matsui
Supervision: S. Braun
Validation: T. Iguchi, S. Lang
Visualization: S. Lang
Writing – original draft: W.-K. Tao
Writing – review & editing: T. Iguchi, S. Lang, K. Mohr, T. Matsui, S. C. van den Heever, S. Braun

ice (snow, graupel, and hail). However, in spite of their importance and links to the dynamical processes, there are few direct measurements of microphysical processes.

Therefore, one of the *key NASA Atmosphere Observing System* (AOS) *Mission's* scientific goals is to examine the relationships between vertical velocities and resulting liquid and ice hydrometeor species. This goal is closely associated with the question posed by the National Academies of Science and Engineering 2017–2027 Decadal Survey (National Academies, 2018), which asks "*Why do convective storms, heavy precipitation and clouds occur exactly when and where they do?*" The AOS Mission will allow us to address such goals through the first ever: (a) global observations of updraft and downdraft convective storm velocities and (b) global collocated observations of the microphysical and dynamical properties of convective cloud systems.

Different methods (instruments) have been used to estimate the vertical velocities in convective cloud systems. For example, the vertical velocity can be estimated from sounding networks (i.e., Houze, 1982; Lin & Johnson, 1996; Yanai et al., 1973). Note that estimating horizontal divergence of air, using a triangular network of rawinsonde stations, was devised by J. C. Bellamy in the late 1940s. However, sounding-estimated vertical velocity is sensitive to the surface or top boundary assumptions. Zhang and Lin (1997) and Zhang et al. (2001) used large-scale analysis to conserve the vertical integration of mass through a constrained variational analysis technique.

Zipser and LeMone (1980) and LeMone and Zipser (1980) statistically analyzed convective updrafts and downdrafts using aircraft data gathered from cumulonimbus cloud penetrations for 6 days during the Global Atmospheric Research Program's Atlantic Tropical Experiment (GATE). They also separated the cloud drafts (used here to collectively indicate updrafts and downdrafts) into active and in-active drafts based on the strength of the vertical velocity. They defined a "draft" to be where the vertical velocity is nonzero continuously for a flight path length of at least 500 m and a "core" to be where the absolute value of the vertical velocity exceeds 1 m s^{-1} for a flight path length of at least 500 m. They found that active updraft velocities were about 2–4 m s^{-1} and active downdraft velocities about −2 to −3 m s^{-1}. They also suggested that the vertical velocity profiles through drafts and cores resemble a "triangle" distribution in which the vertical velocity approached sharply peaked extrema by steady, approximately linear increases and decreases.

Ground-based radar wind profilers can measure the vertical velocity at adequate temporal and high vertical resolutions whereas multiple-Doppler can observe vertical velocity with high spatial coverage within convective cores. Profiler retrievals are reported to have uncertainties to within 1–2 m s^{-1} (e.g., Heymsfield et al., 2010); however, they cannot make direct measurements of air vertical velocities and only measure hydrometeor motions (air vertical velocity plus the reflectivity-weighted fall speed of precipitating hydrometeors). Therefore, the hydrometeor fall speed has to be estimated to obtain air vertical velocity. While fall speed estimates are relatively well-known for some hydrometeors, large uncertainties exist for the denser ice species like graupel and hail. Recently, the combination of radar wind profiler, dual-Doppler (or conventional) radar and field campaign-collected data has been shown to advance the measurement of vertical velocity (i.e., Giangrande et al., 2016; Wang et al., 2019, 2020).

Radar wind profiler, SIPAM (similar to S-band) radar, radiosondes, and disdrometer data were also used to analyze 200 convective events during the Green Ocean Amazon Experiment (GOAmazon) field campaign (Giangrande et al., 2016). The convection classification was based on echo top height, maximum (>35) dBZ without the presence of bright band, and absolute mean Doppler velocity (>5 m s^{-1}) above the freezing level. It also included the weaker echo region aloft. The results show that the mean updraft velocity is about 1 m s^{-1} at low-levels and up to 5 m s^{-1} at the 10-km level while the mean downdraft velocity is less than 1 m s^{-1} at low-levels and 3 m s^{-1} at the 10-km level. The results also show that the convective area frequency of the updrafts is about 7.5% at lower levels but just 2% at the 10-km level, while the frequency of downdrafts is about 10% at the 6-km level and 5% at the lower- and 10-km levels. Wang et al. (2019, 2020) also examined the convective core size and intensity of GOAmazon mature mesoscale convective systems (MCSs) using radar wind profilers. Their results are qualitatively similar to Giangrande et al. (2016). For example, the mean updrafts ($w > 1$ m s^{-1}) are 2 m s^{-1} at low levels and >5 m s^{-1} at upper levels (10 km), and downdrafts ($w < 1$ m s^{-1}) are −2 m s^{-1} at low levels and near 5 m s^{-1} at upper levels.

Tao et al. (1987) used 2D and 3D versions of the Goddard Cumulus Ensemble (GCE) model to investigate the statistical properties of cloud ensembles for a well-organized rain band that occurred during GATE. Tao et al. (1991) also used the GCE model to simulate a subtropical squall line observed during the TAMEX field campaign. The simulated results indicated that the active updrafts with vertical velocity greater than 1 m s^{-1}

account for about 85% of the total upward mass flux budget but only about 10% of the cloud coverage. In contrast, inactive downdrafts with vertical velocities less than 2 m s^{-1} cover a large area and account for more than 60% of the downward mass-flux transport. However, Tao et al. (1987, 1991) used a very small domain and conducted short model integrations. In addition, only warm processes were used in their modeling studies.

In a recent modeling study, Grant et al. (2022) used an ensemble of high-resolution model simulations extending over a wide range of tropical through midlatitude environments, storm types, modes of convective organization, different model platforms and different microphysical schemes, to investigate the relationship between vertical velocity and the conversion of water vapor to condensed water. They found a robust linear relationship between vertical velocity and condensation processes, with the slope of this relationship being first a function of temperature, and second a function of supersaturation. This study clearly indicates the strong links between the microphysical and dynamical processes of convective cloud systems.

In this paper, a numerical cloud ensemble model is used to simulate cloud and precipitation processes associated with two major field campaigns, Dynamics of the Madden-Julian Oscillation (DYNAMO) and GOAamzon. A 15-day and large model domain integration is conducted with sounding derived large-scale advective forcing in temperature and mixing ratio of water vapor from these two field campaigns. These imposed large-scale forcing allow the model to conduct multi-days simulations with reasonable agreement with surface rainfall rate and the vertical structures of apparent heat source (Q_1) and moisture sink (Q_2) (Yanai et al., 1973). Note that the latent heating (LH) is one of the key components of Q_1 and Q_2 (Tao et al., 2010). These imposed large-scale forcing also allow us to simulate cloud and precipitation processes associated with various types of convective clouds and precipitation systems during their respective life cycles. The key objective of the paper is to use the model simulated vertical structure of cloud, precipitation, and the vertical velocity that could facilitate the scientific goals of the AOS Mission. In addition, the LH, cloud/precipitation properties, and vertical velocity (updrafts and downdrafts) will be the key products of the AOS Mission (https://aos.gsfc.nasa.gov), the simulated statistical cloud and precipitation properties will be analyzed. Two specific questions are the focus. The first one is "Where are the specific regions (convective and stratiform region; active and inactive convective core) the LH and cloud properties located/occurred?" and the second is "What are the distributions of LH and cloud properties with respective to the upward and downward direction of the vertical velocity?"

The DYNAMO and GOAmazon case are simulated with the GCE model, including sensitivity tests related to the model resolution (250 vs. 1,000 m) and Goddard microphysical schemes (three-class ice [3ICE] vs. four-class ice [4ICE]). The model, cases and numerical experiments are presented in Section 2. The analysis methodology is described in Section 3. The results are discussed in Section 4, and a summary is presented in Section 5.

2. Model and Cases

2.1. GCE Model and Goddard Microphysics Schemes

The GCE model's advection scheme uses a multi-dimensional Positive Definite Advection Transport Algorithm (Smolarkiewicz & Grabowski, 1990). Solar and infrared radiative transfer processes (Chou & Suarez, 1999; Chou et al., 1999) have been included (Tao et al., 1996). Subgrid-scale (turbulent) processes in the GCE model are parameterized using a scheme based on Klemp and Wilhelmson (1978), and the effects of both dry and moist processes on the generation of subgrid-scale kinetic energy have been incorporated (Soong & Ogura, 1980). In typical multi-day to multi-week integrations, the model has performed reasonably well in terms of surface rainfall, LH profiles and moisture budget structure compared to observations when driven with observed large-scale forcing derived from sounding networks (Soong & Tao, 1980; Tao & Soong, 1986; and many others). Please refer to Tao and Simpson (1993) and Tao et al. (2003, 2014) for more details on GCE model developments and improvements.

The GCE's one moment two liquid and 3ICE microphysics, especially ice processes, have been significantly improved, starting with the reduction of excessive graupel (S. Lang et al., 2007) and unrealistically high reflectivity aloft (S. Lang et al., 2011) and culminating in the new 4ICE scheme (S. E. Lang et al., 2014; Tao et al., 2016). The 4ICE scheme includes parameterizations for rime splintering, immersion freezing, contact nucleation, and a spectral bin microphysics (SBM)-based rain evaporation correction (Li et al., 2009a, 2009b) that reduces excessive evaporation, propagation, and up-shear tilted convective cores. The earlier snow and graupel size-mapping schemes (S. Lang et al., 2011) have been steadily refined (S. E. Lang et al., 2014), including a

snow breakup effect (Tao et al., 2016) to further improve agreement with observed radar PDFs in the ice region. A simple hail size mapping (Tao et al., 2016) eliminates the need to select a hail intercept a priori and produced peak reflectivity profiles dominated by hail in good agreement with NEXRAD observations over a several-hour period for an intense squall line observed over Oklahoma during the Midlatitude Continental Convective Clouds Experiment field campaign (Jensen et al., 2016). The 4ICE scheme has been used to generate the GCE database for the Goddard Convective-Stratiform Heating algorithm (S. E. Lang & Tao, 2018) and Japan Spectral Latent Heating algorithm (Shige et al., 2009), study the land-ocean contrast in tropical convection (Matsui et al., 2016), compared against the SBM scheme for intense convection (Matsui et al., 2019), and evaluated globally in the Goddard Multi-scale Modeling Framework (Chern et al., 2016, 2020; Tao & Chern, 2017). Additional characteristics of Goddard 4ICE scheme are included in Text S1 in Supporting Information S1.

2.2. DYNAMO and GOAmazon

Fifteen-day GCE model simulations for DYNAMO (Equatorial Indian Ocean) and GOAmazon (Amazon Basin) case are conducted. The oceanic case is from the DYNAMO field experiment (13 November to 13 December 2011) that was carried out in the central tropical Indian Ocean to study MJO convective initiation processes and to improve MJO predictions (Yoneyama et al., 2013). Two sounding arrays, together with multiple ground-based radars, provide a rich data set for studying 3D precipitation structures and their associated environment during the MJO onset and mature stage. The current study focuses on the Northern Sounding Array (NSA) for the DYNAMO November MJO event because signals in temporal variations of this MJO event within the NSA are much stronger than in the Southern Sounding Array (Ciesielski et al., 2021; Johnson & Ciesielski, 2013; Johnson et al., 2015; Li et al., 2018). Please see Ciesielski et al. (2021) for more information on large-scale advective forcing used in this study.

The land case selected encompasses the Green Ocean Amazon Experiment or GOAmazon (1 January 2014–31 December 2015). The GOAmazon field campaign provided a wide range of observational resources (including a sounding network) for deployment in the Amazon Basin near Manaus, Brazil. The GOAmazon 2014/2015 campaign has enabled the study of tropical weather and climate processes through the collection of an extensive benchmark data set. The results have been used to improve and validate climate models at a range of scales. Please see Martin et al. (2016). Xie et al. (2004) and Tang et al. (2016) for more information on the GOAmazon field campaign and large-scale forcing derived from the sounding network. GOAmazon is not a typical continental environment because of the high relative humidity.

2.3. Numerical Experiments

Observed large-scale advective tendencies of potential temperature, water vapor mixing ratio, and horizontal momentum were used as the main large-scale forcing in the GCE model in a semi-prognostic manner (Soong & Ogura, 1980; Soong & Tao, 1980; Tao & Soong, 1986). A major characteristic of this approach is that ensembles of clouds can be generated by the "observed-prescribed forcing." The large-scale advective tendencies for potential temperature θ and water vapor mixing ratio q_v,

$$\begin{cases} \left(\dfrac{\partial \overline{\theta}}{\partial t}\right)_l = -\overline{u}\dfrac{\partial \overline{\theta}}{\partial x} - \overline{v}\dfrac{\partial \overline{\theta}}{\partial y} - \overline{w}\dfrac{\partial \overline{\theta}}{\partial z} \\ \left(\dfrac{\partial \overline{q_v}}{\partial t}\right)_l = -\overline{u}\dfrac{\partial \overline{q_v}}{\partial x} - \overline{v}\dfrac{\partial \overline{q_v}}{\partial y} - \overline{w}\dfrac{\partial \overline{q_v}}{\partial z} \end{cases}$$

were derived every 3 hr from the DYNAMO (Equatorial Indian Ocean) and GOAmazon (Amazon Basin) sounding networks (Figure 1). Since accurate calculations of the large-scale horizontal momentum forcing terms are difficult to obtain from observations in the tropics, these terms were instead replaced by a nudging term:

$$\begin{cases} \left(\dfrac{\partial \overline{u}}{\partial t}\right)_l = -\dfrac{\overline{u} - \overline{u}_{\text{obs}}}{\tau} \\ \left(\dfrac{\partial \overline{v}}{\partial t}\right)_l = -\dfrac{\overline{v} - \overline{v}_{\text{obs}}}{\tau} \end{cases}$$

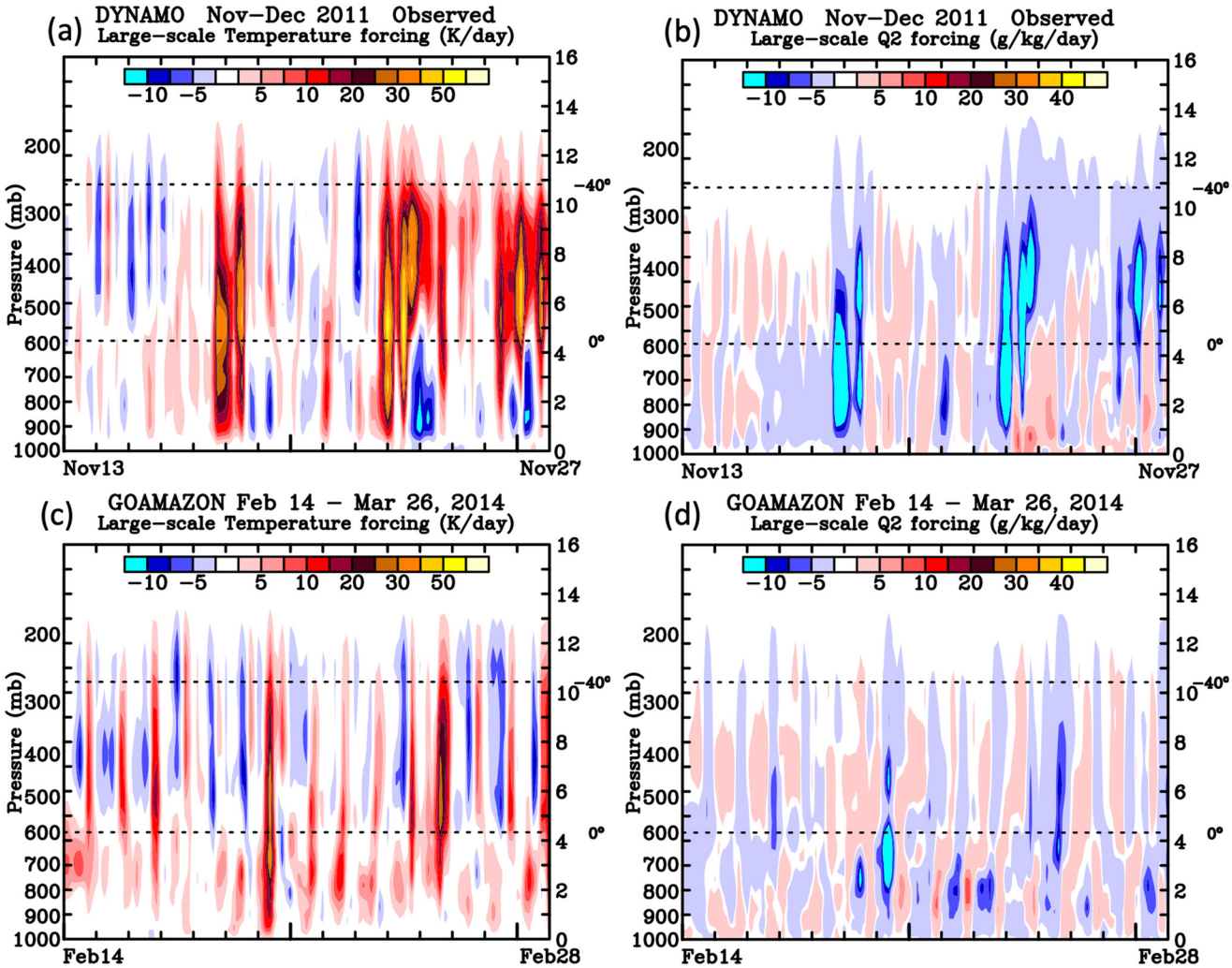

Figure 1. Time series of the large-scale advective forcing in (a) temperature and (b) water vapor derived from the sounding network for the Dynamics of the Madden-Julian Oscillation (DYNAMO) case. Panels (c and d) are same as panels (a and b), respectively, except for the Green Ocean Amazon Experiment (GOAmazon) case. The black dashed lines are domain mean temperature levels at 0°C and −40°C.

where u and v are the model domain averaged wind velocity, u_{obs} and v_{obs} are the observed large-scale horizontal velocity, and τ is the specified adjustment time scale (1 hr). This method constrains the domain-averaged horizontal velocities to follow the observed values, and thereby provides a simple means of controlling the cloud system dynamics by the large-scale momentum and shear. The observed large-scale advective tendencies of potential temperature, water vapor mixing ratio, and horizontal momentum were averaged over the sounding network and provided at 3-hr intervals. Cyclic lateral boundary conditions were incorporated to ensure that there was no additional heat, moisture or momentum forcing inside the domain apart from the large-scale forcing (Soong & Tao, 1980; Tao & Soong, 1986).

The GCE model is run for 15 days, which includes populations of shallow and deep convection, as well as the transition from shallow to deep convection, for both the DYNAMO (13 November–28 November 2011) and GOAmazon (15 February–2 March 2014) cases. Figure 1 shows the large-scale sounding-derived temperature and moisture advective forcing for the DYNAMO (Xie et al., 2004) and GOAmazon cases (Ciesielski et al., 2021). DYNAMO has fewer but larger, longer lasting events while GOAmazon has more numerous, shorter lasting events. Generally, the large-scale temperature forcing is as large as the associated water vapor forcing. In addition, if the large-scale advective forcing is warm (cold), the large-scale forcing in water vapor is dry (moist). The stronger the large-scale forcing in temperature and water vapor, the stronger the convection can typically be.

Table 1
The Eight Experiments Conducted for This Study

	Case	Resolution (m)	Grid points	Microphysics
D4ICE	DYNAMO	1,000	512	4ICE
D4ICEH	DYNAMO	250	2,048	4ICE
D3ICE	DYNAMO	1,000	512	3ICE
D3ICEH	DYNAMO	250	2,048	3ICE
G4ICE	GOAmazon	1,000	512	4ICE
G4ICEH	GOAmazon	250	2,048	4ICE
G3ICE	GOAmazon	1,000	512	3ICE
G3ICEH	GOAmazon	250	2,048	3ICE

Note. Experiment nomenclature, cases (DYNAMO and GOAmazon), horizontal model grid resolution (250 vs. 1,000 m) number of grid points (512 vs. 2,048), and the microphysics parameterization (3ICE vs. 4ICE) for each experiment is shown.

Surface fluxes taken from site-averaged observed fluxes are imposed into the model (Tang et al., 2016) for GOAmazon. Also, for GOAmazon, the surface wind does not interact with the boundary layers. Observed sea surface temperature and the Tropical Oceans Global Atmosphere-Coupled Ocean Atmosphere Experiment surface flux algorithm (Wang et al., 1996) is used to calculate surface fluxes in the DYNAMO case.

A total of eight (two cases) numerical experiments are conducted to examine the sensitivity of model resolution and microphysics (Table 1). The first and second experiments, D4ICE and D4ICEH, are for the DYNAMO case using the 4ICE scheme. The difference between these two experiments is model grid spacing (1,000 m for D4ICE and 250 m for D4ICEH). D3ICE and D3ICEH are the same as D4ICE and D4ICEH, respectively, except the 3ICE scheme is used. The next four experiments, G4ICE, G4ICEH, G3ICE, and G3ICEH are the same as the first four experiments, respectively, except for the GOAmazon case. To have the same model domain size of 512 km, the 250 m resolution experiments require 2,048 total horizontal grid points. The GCE is run 2D for these numerical experiments because it is quite computationally expensive to conduct 3D simulations with a large domain and fine grid spacing over multiple days. The model timestep is 2 s, and there are 80 vertical stretched levels.

3. Analysis Methodology

3.1. Active and Inactive Convective Drafts

In the GCE model simulations, each grid point is designated as either a cloudy or clear point at each integration time, depending upon whether the total liquid and solid water (sum of all cloud hydrometeors) is larger than 0.01 g kg^{-1} at the grid point. The cloudy area can be divided into two parts, cloud updrafts and cloud downdrafts. The cloud updrafts and downdrafts can be subdivided into active and inactive categories. For example, a grid point is designated as an active updraft region if (a) the total liquid and solid water content exceeds 0.01 g kg^{-1} and (b) the vertical velocity is larger than a certain critical value, depending on the definition of "active" at that grid point and at that integration time. Different critical values of 0.5, 1, and 2 m s^{-1} are chosen as shown in Figure 2 (adapted from Tao et al. (1987)). In total, there are four cloudy categories: (a) active updrafts, (b) inactive updrafts, (c) active downdrafts, and (d) inactive downdrafts. The individual contributions of each area to the vertical distribution of LH, vertical velocity and hydrometeors is then quantified. Additional statistics of simulated vertical velocity are presented in Texts S2 and S3 in Supporting Information S1.

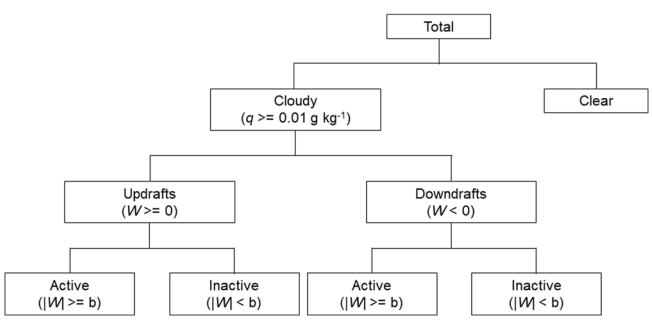

Figure 2. Calibration of clear, active and inactive cloud drafts. The threshold, b, is either 0.5, 1, or 2 m s^{-1}. Adapted from Tao et al. (1987).

3.2. Convective and Stratiform Partitioning Method

In the GCE model convective and stratiform partitioning method, convective, stratiform, and non-surface precipitation regions are identified using information on surface precipitation first. Two additional criteria are applied, which have been included to identify regions where convection may be quite active aloft though there is little or no precipitation at the surface yet, such as areas associated with tilted updrafts and new cells initiated ahead of an organized squall line (Tao & Simpson, 1989; Tao et al., 1993). Non-surface precipitation regions are considered to be convective if the sum of cloud water and cloud ice exceeds a certain threshold (i.e., 0.5 g kg^{-1}) or if the updraft exceeds a certain threshold (i.e., 3 m s^{-1}) below the melting level. The presence of this amount of cloud water/cloud ice is a good indication of a saturated area (100% relative humidity). This method has been adapted in other CRMs (Alexaner & Cotton, 1998; Chin, 1994; Redelsperger et al., 2000). S. Lang et al. (2003) reviewed and tested different convective and stratiform separation techniques using the GCE.

3.3. Probability Vertical Distribution

GCE-simulated clouds and cloud systems contribute to mass, sensible heat, moisture transport, and latent heat release via condensation, deposition, and freezing, and latent heat absorption via sublimation, evaporation, and melting. These cloud transport and microphysical processes are divided into distributions consisting of 25 categories of cloud updrafts and 10 categories of cloud downdrafts. The interval between each category is 1 m s^{-1}. The properties of GCE-simulated clouds/cloud systems in each distribution interval with respect to different convective activities or different strengths of cloud drafts can be analyzed. This approach follows a similar methodology previously performed by Tao et al. (1987). However, their study is based on a much earlier version of the GCE model in which ice processes and radiation were not considered. Their study was also conducted over very short integrations using much more limited model domain sizes. Nevertheless, their results indicated that there is very good correlation between cloud updraft mass fluxes and condensation rates. The results also indicated that there is a strong correlation between cloud downdraft mass fluxes and evaporation rates (see Figure 10 in Tao et al., 1987).

4. Results

4.1. Surface Rainfall

There is good agreement in the temporal variation of surface rainfall rates between the GCE model simulated precipitation and that estimated using the sounding network for both the DYNAMO and GOAmazon cases (Figure 3). The agreement is due to the fact that the sounding-estimated large-scale tendencies in temperature and water vapor mixing ratio are imposed on the model temperature and water vapor fields (this approach is sometimes called a semi-prognostic approach, see Soong & Tao, 1980; Tao & Soong, 1986; and many other CRM studies). When the imposed large-scale advective forcing cools and moistens the environment, the model responds by producing clouds through condensation and deposition. The fallout of large, mm- or greater, precipitation particles produce rainfall at the surface when these ice particles fall to low levels and then melt. The larger the advective forcing, the larger the microphysical response (rainfall) the model will produce. This is clearly shown in two very active convective periods (18 and 23 November) for the DYNAMO case (Figure 3a). On the other hand, the model will not produce any clouds or rainfall when the imposed large-scale advective forcing heats and dries the atmosphere. For GOAmazon, most of the convective events are weaker than those during the active phases in DYNAMO.

Figures 4a and 4b show the temporal and spatial variation GCE-simulated surface rainfall rates for the D4ICEH and G4ICEH runs. There are three major simulated precipitation events with higher and longer lasting surface rain rates compared to the other DYNAMO precipitation events. One of the precipitation events (23–25 November) has the strongest precipitation in both total rainfall amount and precipitation rate. By contrast, the G4ICEH run produced many more simulated precipitation events but with relatively shorter life cycles compared to the three simulated D4ICEH November events. Three stronger precipitation events did occur during and around 15, 22, and 26 February. The area of the convective and stratiform regions in the DYNAMO and GOAmazon cases is shown in Figures 4c and 4d. The convective area is coincident with large rainfall rates for both cases. In addition, the stratiform area is usually associated with the convective area but has a time lag and/or is behind the convective region. There is more stratiform area in the DYNAMO case than in the GOAmazon case.

Note that the model simulated a population of different types of clouds and convective systems over their respective life cycles in both cases. In both cases, there are many small convective precipitating events that appear to be "stratiform cloud" but are really weak or decaying convection. These small convective precipitating events result from our convective-stratiform separation method that also considers the vertical velocity.

Table 2 shows the model simulated total surface rainfall and their associated convective and stratiform components, including the stratiform percentage, for all eight cases. The DYNAMO simulations produce more total rainfall and have higher stratiform rainfall percentages than their GOAmazon counterparts. The higher rainfall is caused by larger advective temperature and water vapor forcing in DYNAMO than in GOAmazon (Figure 1). Generally, the model grid spacing, and microphysics do not affect the total surface rainfall rate (less than 1% difference) for both DYNAMO and GOAmazon. The D3ICE and G3ICE (using 1,000 m grid spacing and the 3ICE scheme) simulations have about 2% more stratiform rain than their corresponding 4ICE experiments. The high-resolution simulations have slightly smaller stratiform rainfall amounts (~2 to 4 mm) as well as stratiform

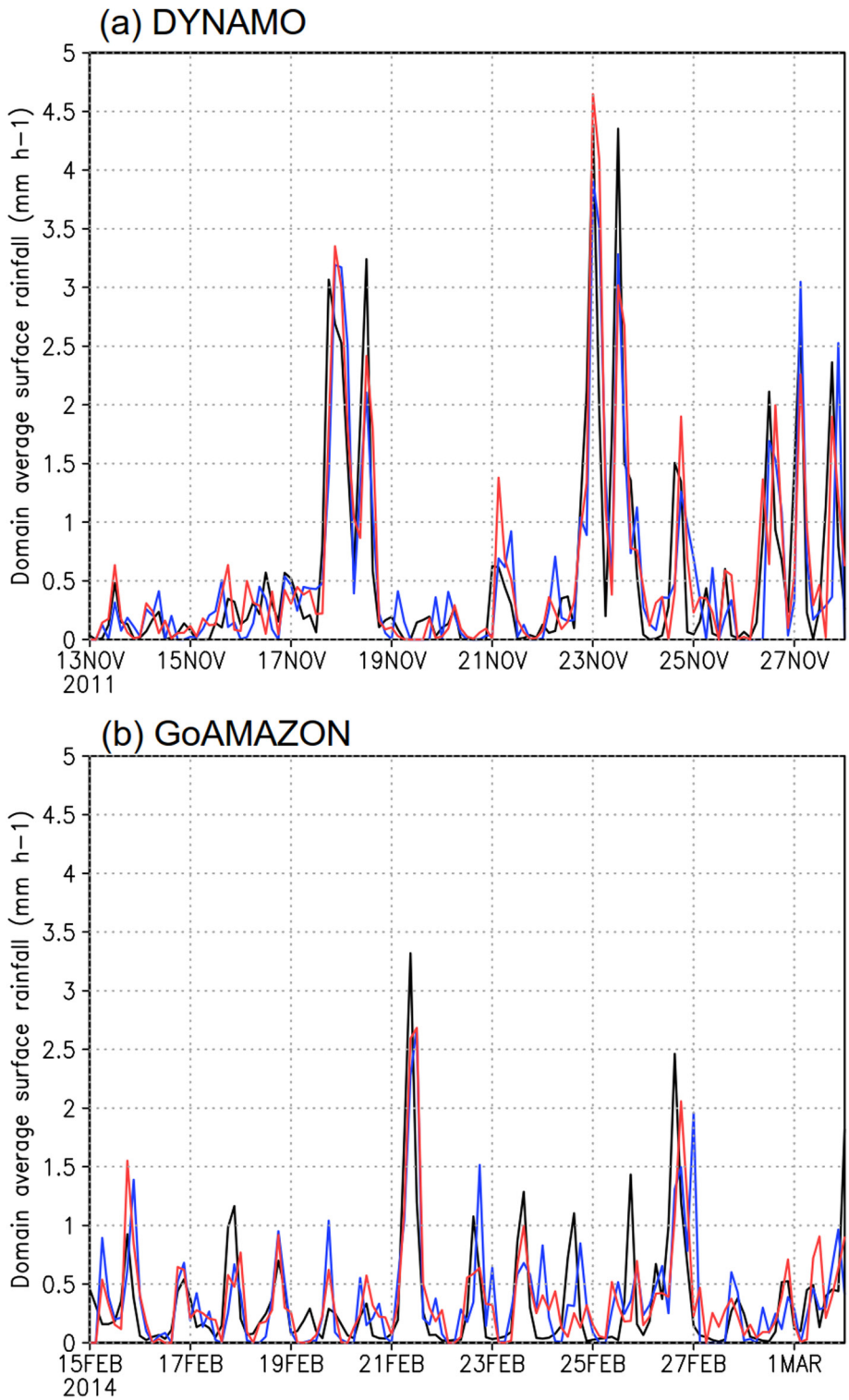

Figure 3. Time series of 2D Goddard Cumulus Ensemble-simulated domain average surface rainfall using 1 km (blue) and 250 m horizontal resolution (red) with 4ICE versus surface rainfall derived from the corresponding sounding budget (black) for the (a) Dynamics of the Madden-Julian Oscillation (DYNAMO) and (b) Green Ocean Amazon Experiment (GOAmazon) cases. Units are in mm h^{-1}.

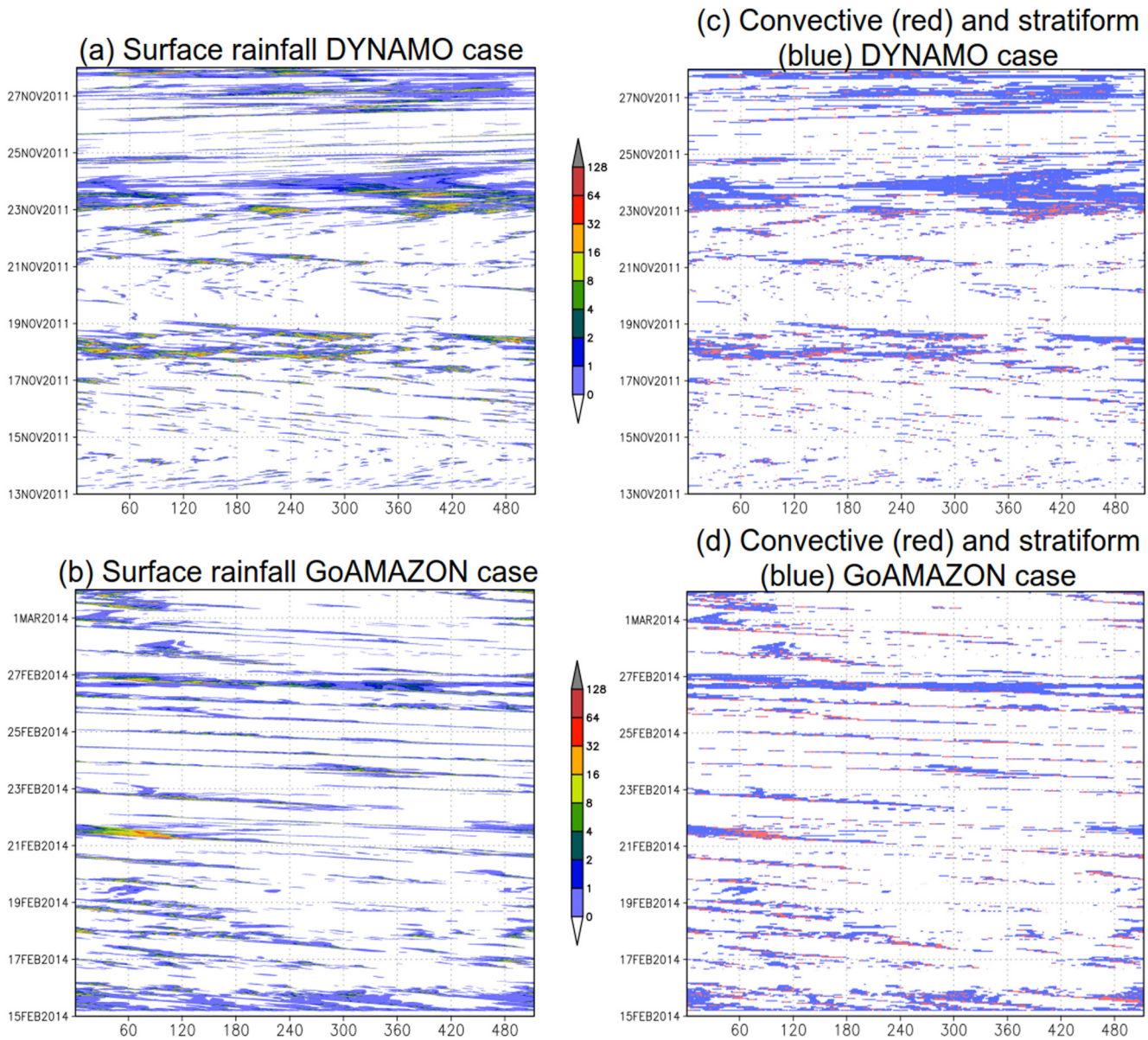

Figure 4. Horizontal distribution of surface rainfall rate (mm h^{-1}) versus time (Hovmoller diagram) for the 2D 4ICE simulations with 250 m model resolution for the (a) Dynamics of the Madden-Julian Oscillation (DYNAMO) (D4ICEH) and (b) Green Ocean Amazon Experiment (GOAmazon) (G4ICEH) cases. Panels (c and d) is the area covered by the convective (red) and stratiform (blue) region for the DYNAMO and GOAmazon case, respectively.

percentages (~0.5% to 1.5%) compared to those with coarse resolution for both the DYNAMO and GOAmazon cases.

All of the results presented in the following sections are based on in-line statistics that are calculated and stored every minute within the model runs and accumulated over the entire 15-day model integrations for all of the DYNAMO and GOAmazon simulations. These cloud statistics include many different types of cumulus clouds at different stages of their lifecycles (as shown in Figure 4). Since the differences in surface rainfall and its stratiform percentage (Table 2) is quite small between the cases with different grid spacing and microphysics, the high-resolution cases with the 4ICE scheme (D4ICEH and G4ICEH) will be presented when describing the LH and hydrometeor distributions in Section 4.2 and 4.3. Sensitivity to the model grid spacing and microphysics scheme will be examined in later sections (Section 4.4 and 4.5). Sections 4.2, 4.3 and 4.4 focus on vertical profiles and Section 4.5 on vertically integrated cloud properties.

Table 2
Total, Convective, and Stratiform Simulated Rainfall for the DYNAMO and GOAmazon Cases

	Total rain (mm)	Convective rain (mm)	Stratiform rain (mm)	Stratiform percentage (%)
D4ICE	204.22	118.33	85.89	42.06
D4ICEH	201.79	118.63	81.16	41.21
D3ICE	202.06	113.63	88.52	43.76
D3ICEH	201.03	116.21	84.82	42.19
G4ICE	129.47	85.80	43.67	33.73
G4ICEH	128.14	86.72	41.42	33.32
G3ICE	128.20	82.53	45.67	35.62
G3ICEH	128.98	85.83	43.15	33.45

Note. Sounding estimated rainfall is 119.36 and 197.85 mm for the GOAmazon and DYNAMO case, respectively.

4.2. Vertical Velocity Versus Latent Heating

There are six LH terms represented in the model that correspond to the six phase changes of water substance: condensation (heating from water vapor to cloud water), evaporation (cooling from cloud water and raindrops to water vapor), deposition (heating from water vapor to cloud ice), sublimation (cooling from cloud ice, snow, graupel, and hail to water vapor), freezing (heating from cloud water/raindrops to graupel and hail), and melting (cooling from snow, graupel, and hail to raindrops). Note that the results are from many convective and precipitating clouds of different sizes and at different stages of development. LH profiles are quite different in the convective and stratiform regions of "mature" convective/precipitation systems (e.g., Houze, 1982; Johnson, 1984). Warming via condensation and deposition (and freezing) dominates throughout the column in the convective region. However, in the stratiform region, warming (heating) occurs above the melting level through deposition, while cooling, mainly from evaporation, prevails beneath the melting level. Therefore, simulated vertical LH profiles are separated into convective and stratiform regions, and their relationships with vertical velocity are examined. In this and the following sections, almost all results from the high-resolution (i.e., smaller grid spacing), 4ICE parameterization simulations (D4ICEH and G4ICEH) will be analyzed and discussed.

There is a very similar distribution between DYNAMO and GOAmazon in terms of heating and cooling in the convective region. The vertical velocity is binned over 1 m s^{-1} intervals for downdrafts (0 to −10 m s^{-1}) and updrafts (0–25 m s^{-1}). Condensation and deposition mainly occur in the updraft region (Figures 5a, 5c, and 6c). Condensation heating occurs in association with vertical velocities up to 10 m s^{-1}, and it is found mainly beneath the −10°C level. Deposition occurs in a range that includes stronger vertical velocities but is found mainly above the freezing (0°C) level. Both evaporative and sublimational cooling (Figures 5b, 5d, and 6d) are found in association with weak and moderate downdrafts (~1 to 5 m s^{-1}). Evaporative cooling occurs near and beneath the freezing level, while sublimational cooling is found above (higher up) this level. Stronger downdrafts (3–5 m s^{-1}) are usually associated with larger evaporative and sublimational cooling. There is weak evaporative and sublimational cooling (~0.1 g kg^{-1} h^{-1}) associated with weaker updrafts due to entrainment near cloud boundaries. Both melting and freezing (Figures 5e, 5f, and 6f) occur in strong updraft (10 m s^{-1}) and downdraft (~5 m s^{-1}) regions and are located mainly within a relatively narrow region (about 2 km in depth) compared to the other LH terms. Strong freezing (heating) occurs above the 0°C level in the updraft region while strong melting (cooling) occurs beneath the 0°C level in the downdraft region. Also note that the contribution of the melting and freezing to the total LH is smaller than the condensation, evaporation, deposition, and sublimation primarily because the latent heat of fusion is one order of magnitude smaller than the latent heat of condensation and sublimation.

In spite of their similarities, there are notable differences between the DYNAMO and GOAmazon cases. One major difference is that less condensation occurs in the updraft region, and especially so in the strong updraft region (i.e., 10 m s^{-1} or stronger), in the GOAmazon case. However, compared to DYNAMO, deposition in GoAmazon is larger and occurs in the stronger updraft regions. In addition, there is less evaporation but more sublimation in the downdraft region (Figures 6b and 6d) of GOAmazon compared to DYNAMO. Both deposition and sublimation occur in the high velocity regions (i.e., >10 m s^{-1} for deposition and <−5 m s^{-1} for sublimation) for the GOAmazon case. Both freezing and melting occur in the updraft and downdraft regions (Figures 6e and 6f) of GOAmazon as in DYNAMO. However, they are much weaker compared to DYNAMO.

In the stratiform regions, the distribution of heating and cooling is also similar between the DYNAMO and GOAmazon cases. There is large low-level condensational heating in the stratiform regions (Figures 7a and 8a); this heating is due to shallow convection being identified as stratiform in the convective-stratiform algorithm as opposed to processes occurring in direct association with a storm anvil. Large depositional heating (Figures 7c and 8c) can occur in very weak updrafts (less than 1–2 m s^{-1}). Both evaporative and sublimational cooling are mainly associated with the downdraft regions (Figures 7b, 7d, and 8d). Strong sublimational cooling extends to higher altitudes in the stratiform cloud regions compared to that in the convective regions. The strong evaporative

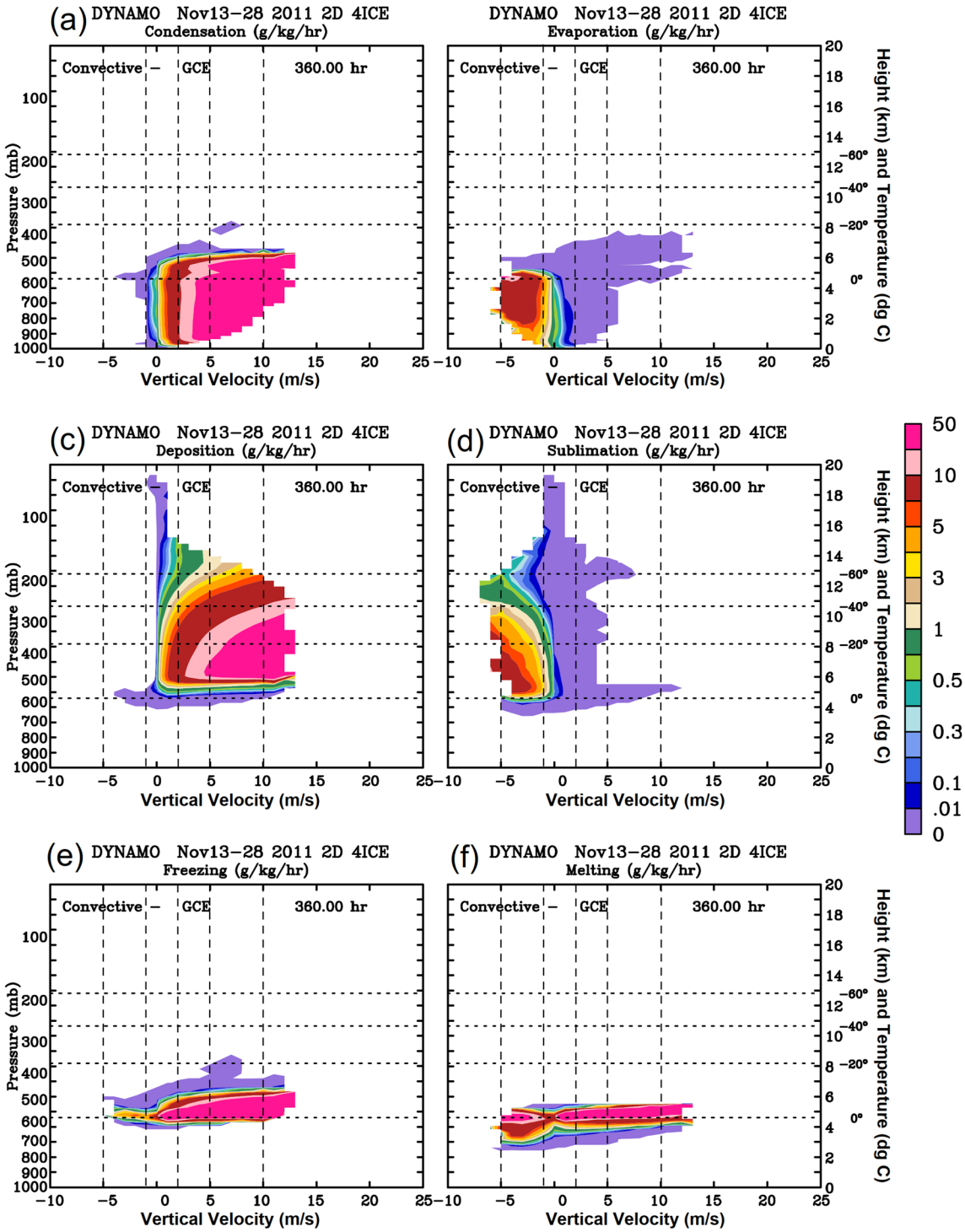

Figure 5. The distribution of the mean (a) condensation rate, (b) evaporation rate, (c) deposition rate, (d) sublimation rate, (e) freezing rate, and (f) melting rate with respect to cloud vertical velocity as a function of height for the Dynamics of the Madden-Julian Oscillation (DYNAMO) convective region. Evaporation, sublimation and melting result in cooling; condensation, deposition, and freezing result in heating. The vertical dashed lines are the vertical velocity at −5, −1, 2, 5, and 10 m s^{-1}. The horizontal dashed lines are the domain mean temperature levels. The color scale shows values divided by the ranges of 0, 0.1, 0.2, 0.3, 0.4, 0.5, 0.75, 1, 2, 3, 4, 5, 7.5, 10, 30, and 50, corresponding to the color bar.

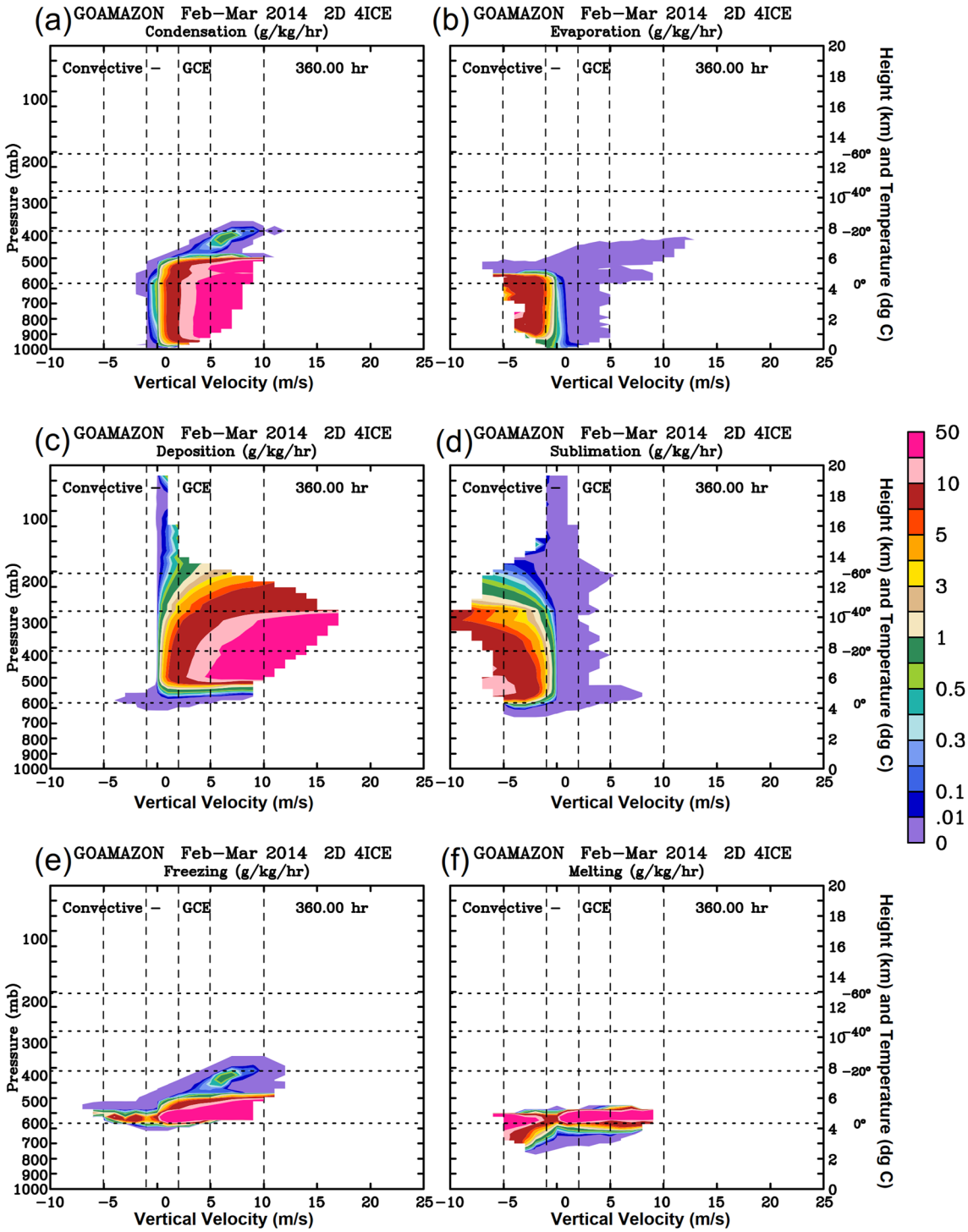

Figure 6. Same as Figure 5 except for the Green Ocean Amazon Experiment (GOAmazon) case.

cooling in the stratiform regions is associated with weak and moderate downdrafts (−2 to −4 m s^{-1}) and beneath the freezing level similar to the convective regions.

One major difference in the freezing and melting between the convective (Figures 5e, 5f, and 6f) and stratiform (Figures 7e, 7f, and 8f) regions is that very low freezing and melting rates occur in the updrafts of the stratiform regions. Condensation heating only occurs in the relatively weak updraft regions for GOAmazon compared to the

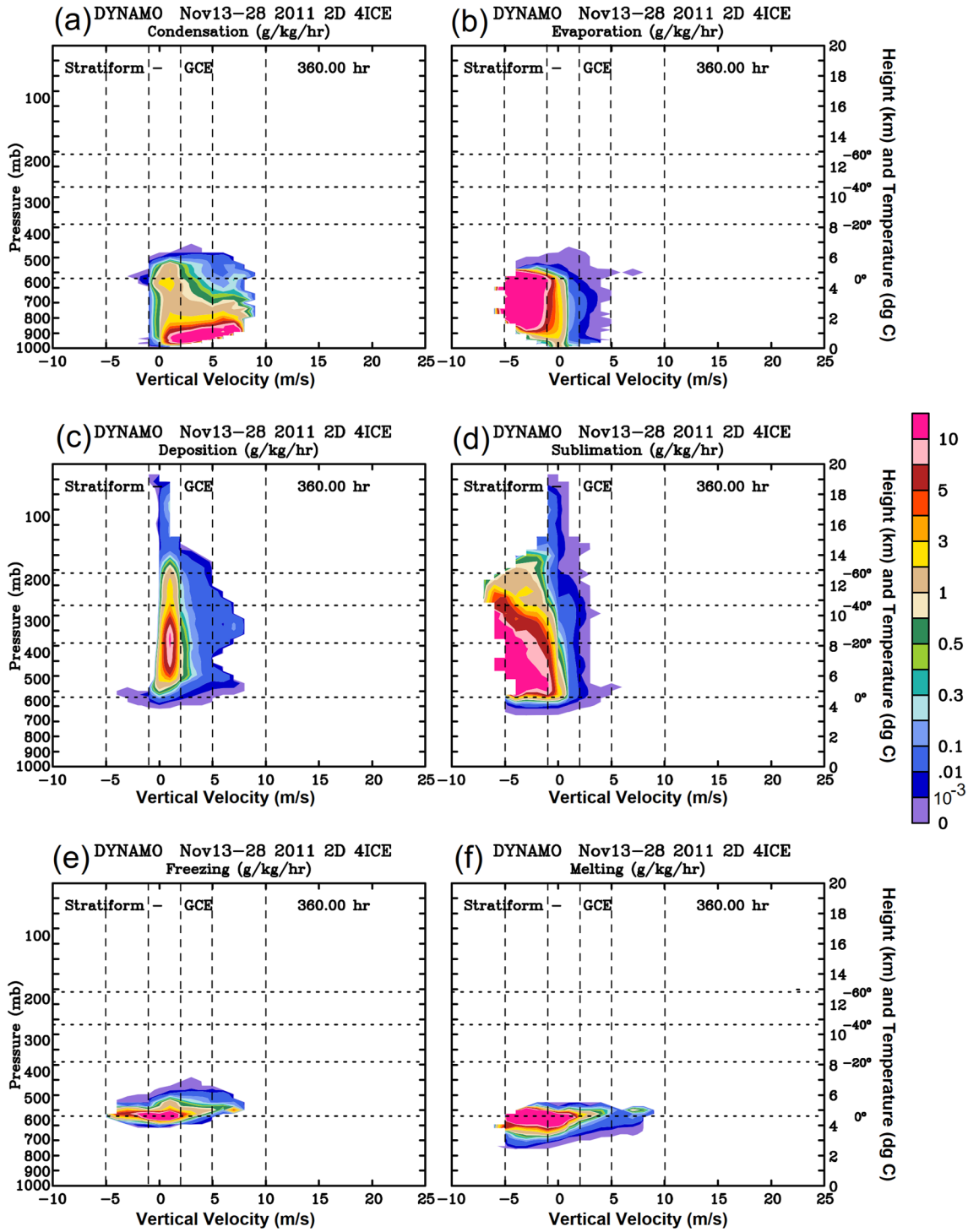

Figure 7. Same as Figure 5 except for the stratiform regions. The color scale shows values divided by the ranges of 0, 0.001, 0.01, 0.1, 0.2, 0.3, 0.4, 0.5, 0.75, 1, 2, 3, 4, 5, 7.5, and 10 corresponding to the color bar.

DYNAMO stratiform region. Evaporative cooling is also weaker, while sublimational cooling is stronger in the GOAmazon case compared to DYNAMO. Deposition, freezing, and melting rates are slightly weaker compared to their DYNAMO counterparts. One possible explanation is that the vertical velocities are weaker in GOAmazon than in DYNAMO (shown in Section 4.4).

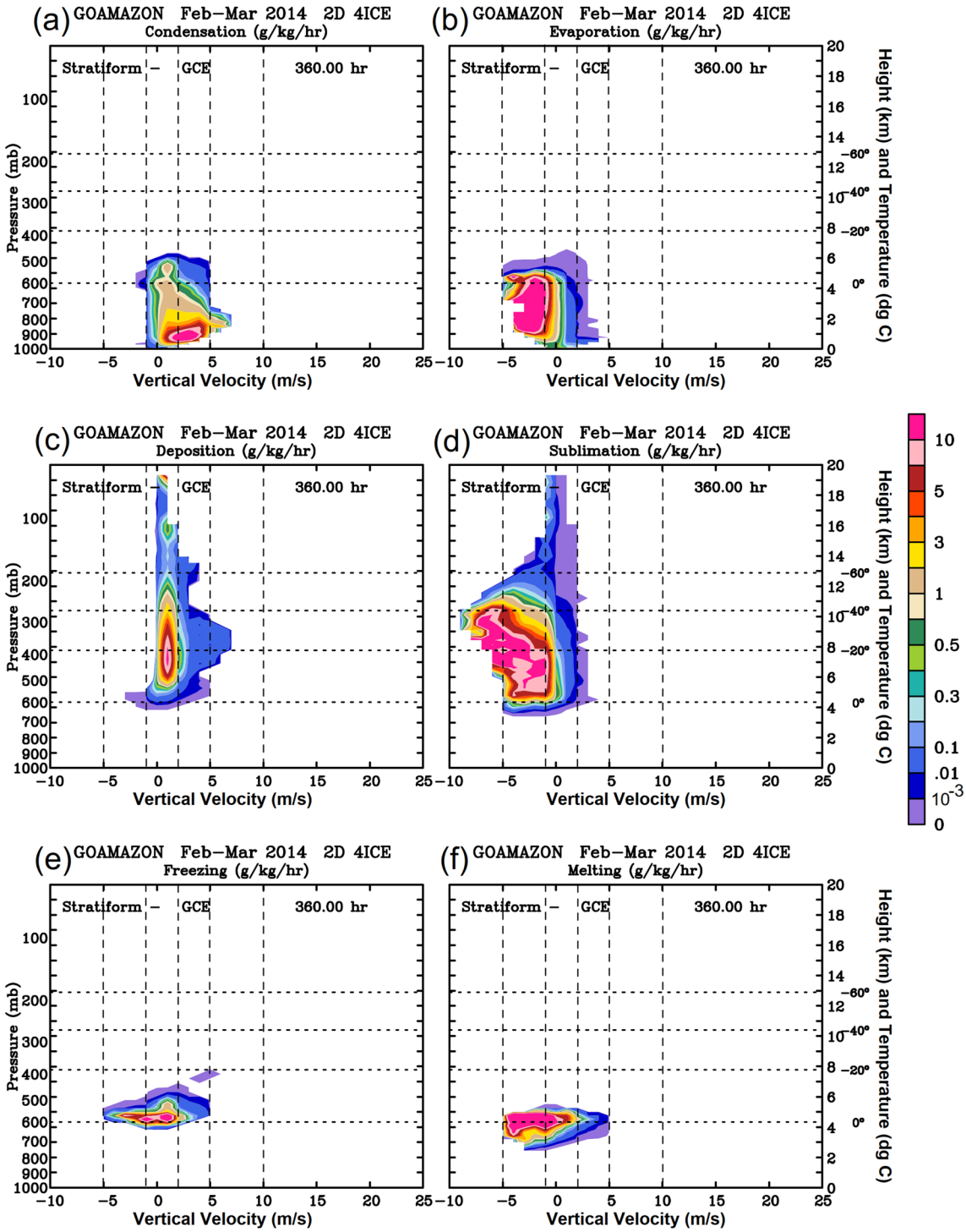

Figure 8. Same as Figure 6 except for the stratiform region.

4.3. Vertical Velocity Versus Cloud Properties (Cloud Water, Rain, Cloud Ice, Snow, Graupel, and Hail)

There are some interesting similarities and differences between the distribution of cloud hydrometeors with respect to the cloud updrafts and downdrafts between the GOAmazon and DYNAMO cases. In the convective region, both cases show that more cloud water (Figures 9a and 10a), rain (Figures 9b and 10b), cloud ice (Figures 9c and 10c), and hail (Figures 9f and 10f) occur in the updrafts, whereas snow (Figures 9d and 10d)

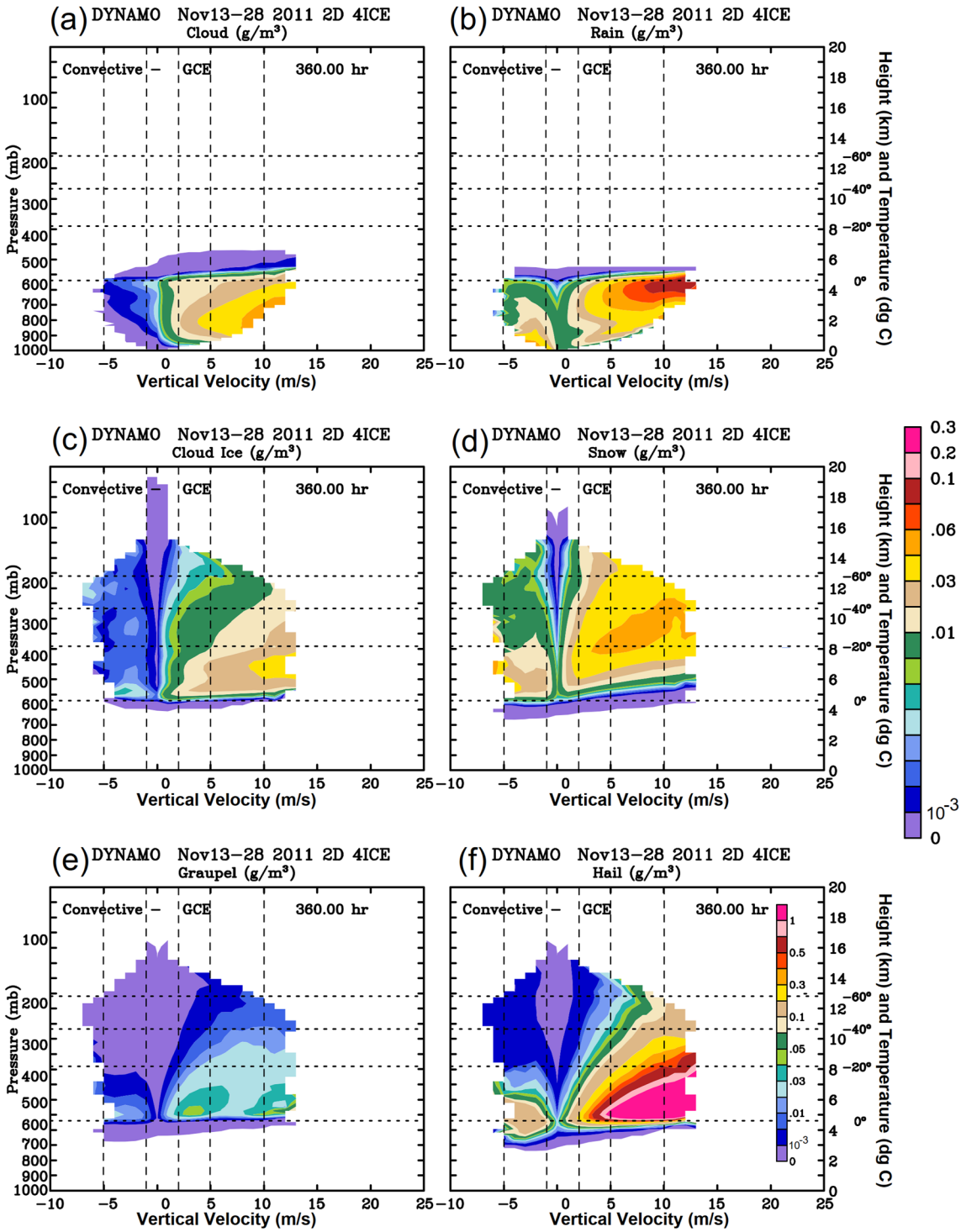

Figure 9. The distribution of mean (a) cloud water, (b) rain, (c) cloud ice, (d) snow, (e) graupel, and (f) hail content with respect to the cloud vertical velocity for the Dynamics of the Madden-Julian Oscillation (DYNAMO) convective region. Units are in g/m^3. The vertical lines are the vertical velocity at −5, −1, 2, 5, and 10 m s^{-1}. Note that the color bar for the hail is not the same as the other hydrometeors. Hail is more concentrated in strong updraft parts than others. The color scale shows values divided by the ranges of 0, 0.001, 0.002, 0.003, 0.004, 0.006, 0.008, 0.01, 0.02, 0.03, 0.04, 0.06, 0.08, 0.1, 0.2, and 0.3 corresponding to the color bar, except for the panel of hail; the ranges in the hail panel are 0, 0.001, 0.0075, 0.01, 0.02, 0.03, 0.04, 0.05, 0.075, 0.1, 0.2, 0.3, 0.4, 0.5, 0.75, and 1.

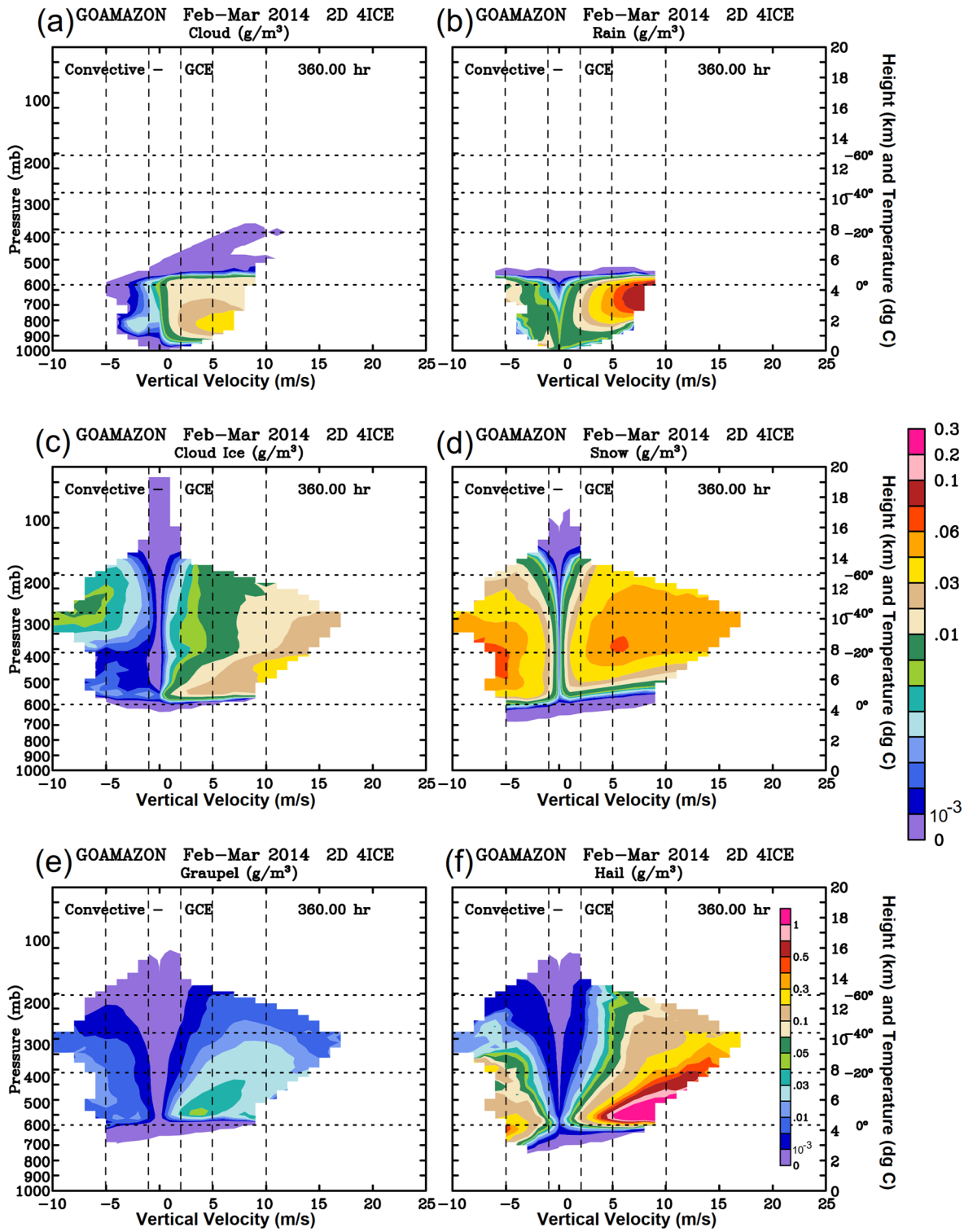

Figure 10. Same as Figure 9 except for the Green Ocean Amazon Experiment (GOAmazon) case.

and graupel (Figures 9e and 10e) occur in both the updraft and downdraft regions, with less graupel than snow. Both snow and graupel can occur in strong updrafts (>10 m s^{-1}) as well as strong downdrafts (<5 m s^{-1}). Hail (Figures 9f and 10f) mainly occurs in strong updrafts (>5 m s^{-1}) at middle levels (from 0°C to −20°C). The color bar for hail is not the same as the other hydrometeors shown in Figures 9 and 10; hail is present mainly in the

strong updraft regions (>5 m s^{-1}). For oceanic cases such as DYNAMO, hail is observed much less frequently compared with continental cases. However, in the 4ICE scheme, the hail category includes both small frozen drops and large hail as normally defined in observations. These small frozen drops may largely explain the amount of hail simulated, located mainly near the freezing level. The other possible reason is the limitation inherent in the one-moment bulk microphysical scheme where the low cloud condensation nuclei number concentration in the oceanic environment cannot be explicitly represented.

However, there is less cloud water and rain in the relatively strong updraft (>7 m s^{-1}) and downdraft (−4 m s^{-1}) regions for the GOAmazon case. This is because both the condensation and evaporation rate distributions are also narrow in the GOAmazon case (see Figures 5 and 6). Another difference between the cases is that very small cloud water amounts occur at the 10°C level, and there is more rainwater at low levels in the weak downdraft region (∼−1 m s^{-1}) for GOAmazon. The cloud ice, snow, graupel, and hail distributions are also wider (also deeper) with respect to the vertical velocity (i.e., exist in both strong updrafts and downdrafts) compared to those in the DYNAMO case.

In the stratiform regions, there are also some similarities between the GOAmazon and DYNAMO cases. Both have small amounts of low-level cloud water (Figures 11a and 12a) and rain (Figures 11b and 12b) in the updraft regions. All ice species (cloud ice [Figures 11c and 12c], snow [Figures 11d and 12d], graupel [Figures 11e and 12e], and hail [Figures 11f and 12f]) are mainly within the downdraft regions and above the freezing level, but there is cloud ice and snow present in the very weak updraft regions in both cases. But all GOAmazon cloud water, rain, cloud ice, and graupel mixing ratios are smaller than their DYNAMO counterparts. The smaller amount of cloud water and rain in the former is due to the smaller condensation and evaporation rates in the GOAmazon case (Figures 6a and 6b) versus in the DYNAMO case (Figures 5a and 5b). There is hail in both the updraft and downdraft regions (Figures 11f and 12f), though more hail occurs in the downdraft region. The hail above the freezing level in the updrafts are due to drops freezing while the larger amounts of hail in the stronger downdrafts that extend well above the freezing level are due to the detrainment from the updraft cores.

There are similar distributions (shapes) between the LH and hydrometeors in both the convective and stratiform regions for both cases. In the convective updraft regions, the structures (shapes) of the cloud water and cloud ice distributions are quite similar to the condensation and deposition, respectively, as shown in Figures 5a and 6a. The large cloud water mass (yellow color in Figures 9a and 10a) is closely associated with large condensation rates (pink color in Figures 5a and 6a). Rainwater in the downdraft region has a similar structure to the evaporation rates (Figures 5b and 6b). Melting (Figures 5f and 6f) can contribute to rainwater formation near and beneath the freezing level in both updraft and downdraft regions. It is interesting to note that there are large rainwater amounts in the updraft regions. This rainwater formation is mainly associated with melting processes. The rain terminal velocity could be stronger than the convective updrafts, and consequently, rain could fall from the freezing level to lower levels in the updraft region. In addition, cloud ice (Figures 9c and 10c) has a very similar structure (or shape) to the deposition rate in the convective updraft region (see Figures 5c and 6c). There are large cloud ice contents and deposition rates above the freezing level and beneath the 200 hPa level. The relatively small cloud ice content (less than 0.01 g m^{-3}) in the downdraft region could be caused by detrainment from the deep convective core regions.

In the stratiform region, cloud water (Figures 11a and 12a) has a similar structure to the condensation rate (Figures 7a and 8a). This is a result of the weak, shallow convection being identified as stratiform by the convective-stratiform partitioning algorithm. However, there are some small cloud water amounts without corresponding condensation in the downdraft region. This feature is also found in the convection region. Rainwater in the stratiform region (Figures 11b and 12b) occurs in the weaker downdraft region (<3 m s^{-1}) where large evaporation rates also occur (Figures 7b and 8b). There is rainwater in the updraft region that could be caused by shallow convection (especially with low cloud tops ∼2 to 3 km height).

4.4. Active Versus Inactive Cloud Properties and the Role of Latent Heat Release

LH and cloud hydrometeors are also calculated in the cloudy, active and inactive cloud drafts (upward and downward motions) based on Figure 2. Two "*b*" values are selected for active updrafts and downdrafts. For the active updraft areas, 1 and 2 m s^{-1} are selected, while −0.5 and −1.0 m s^{-1} are selected for active downdrafts. Note that the same values for downdrafts were used in previous observational (Zipser & LeMone, 1980)

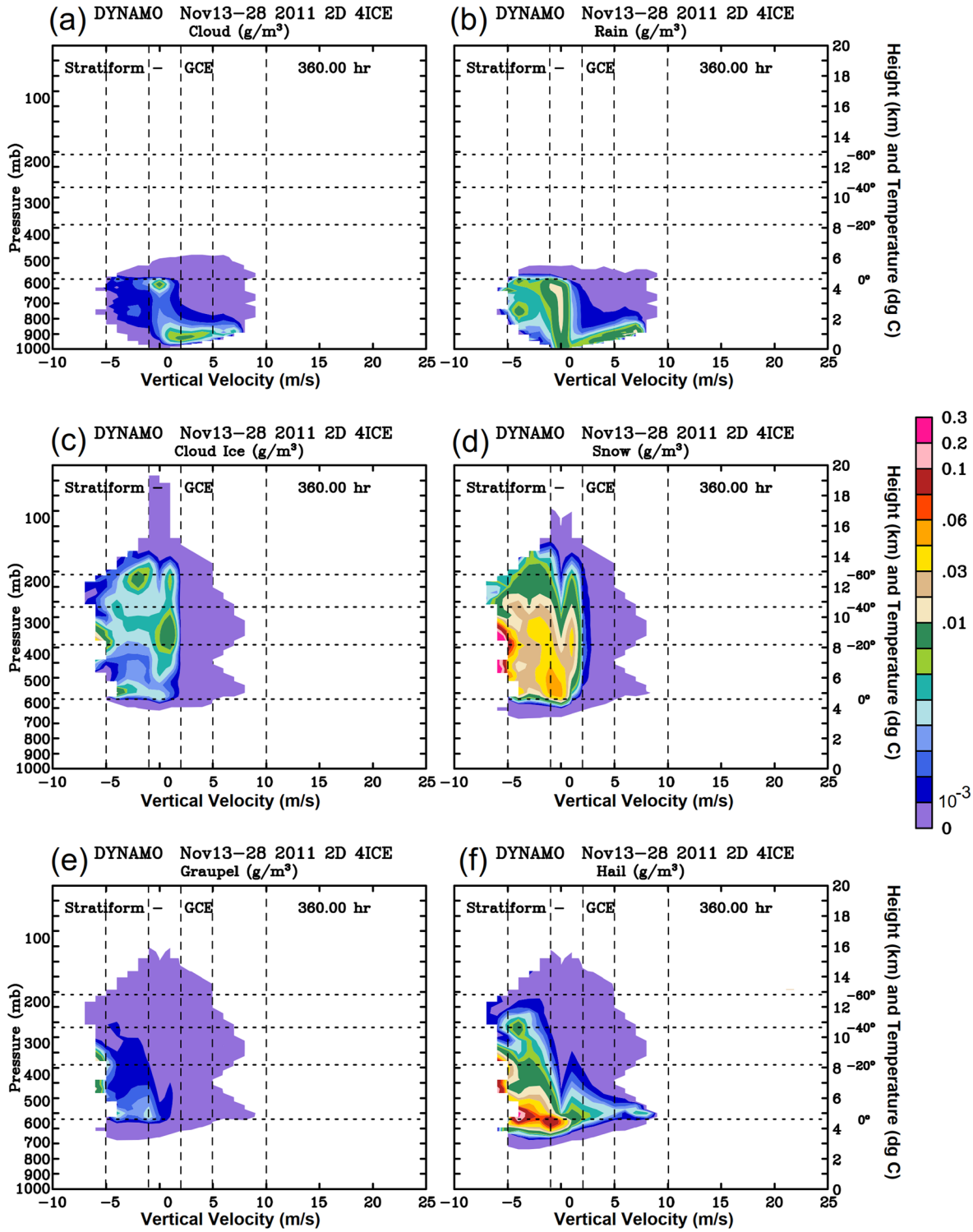

Figure 11. Same as Figure 9 except for the stratiform regions. The color scale shows values divided by the ranges of 0, 0.001, 0.002, 0.003, 0.004, 0.006, 0.008, 0.01, 0.02, 0.03, 0.04, 0.06, 0.08, 0.1, 0.2, and 0.3, corresponding to the color bar in all panels.

and modeling studies (Tao et al., 1987). The values for updrafts were smaller (0.5 and 1 m s^{-1}) in Zipser and LeMone (1980). The cloud statistics include many different types (i.e., shallow, deep) of clouds in different life cycles of convective-precipitation systems (see Figure 4). The smaller values used for the active downdrafts is because downdrafts are usually weaker than updrafts.

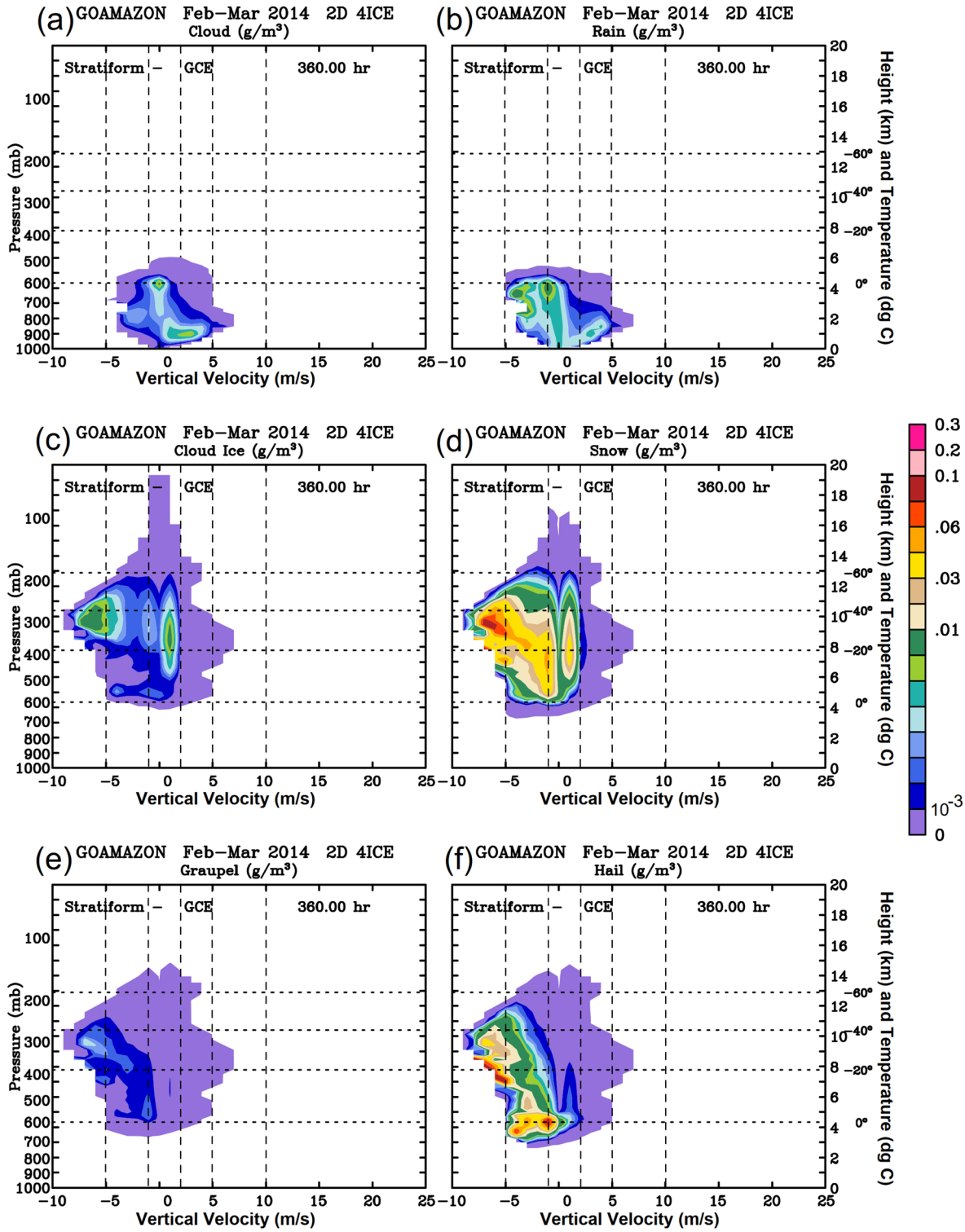

Figure 12. Same as Figure 10 except for the stratiform region.

The area coverage of active updrafts and active downdrafts is shown in Figure 13. The fractional area coverage of active updrafts with an absolute vertical velocity exceeding 1 or 2 m s^{-1} is only 0.5%–1.2% of the total domain, respectively, for the DYNAMO case. Active downdrafts cover more area than active updrafts (Figure 13a). Active updrafts are usually located in the convective region, while active downdrafts are in the lower levels of the

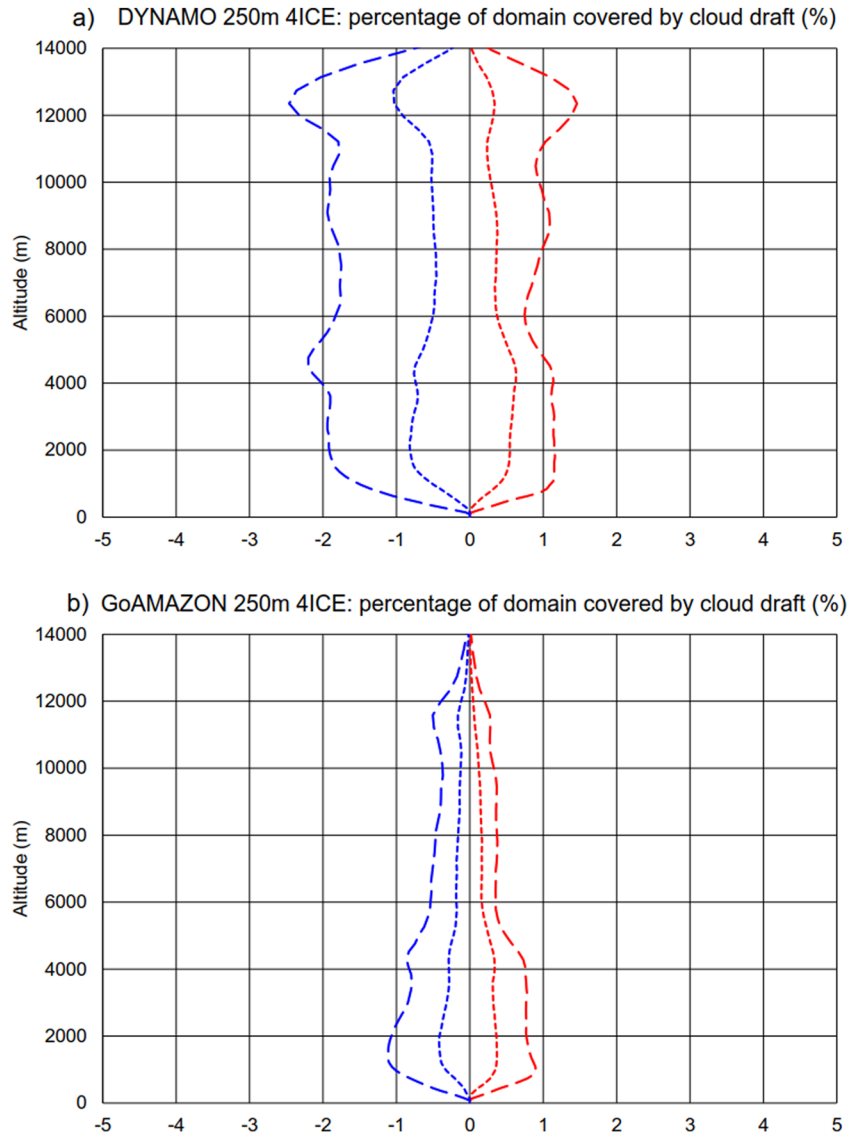

Figure 13. Percent of domain covered by updraft (red lines) and downdraft (blue lines) areas over the whole domain: shown are active updraft and downdraft areas where the absolute vertical velocity exceeds 1 (long-dashed lines) or 2 (short-dash lines) m s^{-1} for updrafts and 0.5 (long-dashed lines) and 1 (short-dashed lines) m s^{-1} for downdrafts. The 2 (1) m s^{-1} group is a subset of the 1 (0.5) m s^{-1} group for updrafts (downdrafts). Panel (a) is for the Dynamics of the Madden-Julian Oscillation (DYNAMO) (D4ICEH) and (b) the Green Ocean Amazon Experiment (GOAmazon) (G4ICEH) case.

stratiform region. The stratiform aerial coverage is greater than the convective areal coverage (Figure 4b). For the GOAmazon case (Figure 13b), the fractional area coverage of active cloud drafts with an absolute vertical velocity exceeding 0.5 or 1 m s^{-1} is relatively small (less than 1.2% of the total domain). There are more active updrafts and downdrafts in the DYNAMO case than in the GOAmazon case. More total surface rain and convective rain in DYNAMO compared to GOAmazon (see Table 2) accounts for this difference. LeMone and Zipser (1980) and Zipser and LeMone (1980) showed that the area coverage by active drafts (cores) is only a few percent from 0.3 near the surface to 2% at middle levels to 4% at upper levels for updrafts with the area coverage for active downdrafts (cores) about half of that for active updrafts (cores). The current modeling results show less area coverage (about 0.5% and 2% in the low and upper troposphere) than these prior observations. Recently, Wang et al. (2019, 2022) showed that the convective area frequency of the updrafts is about 7.5% at lower levels but just 2% at the 10-km level, while the frequency of downdrafts is about 10% at the 6-km level and 5% at the lower- and 10-km levels for GOAmazon mature MCS. Our results show less area coverage than the observation.

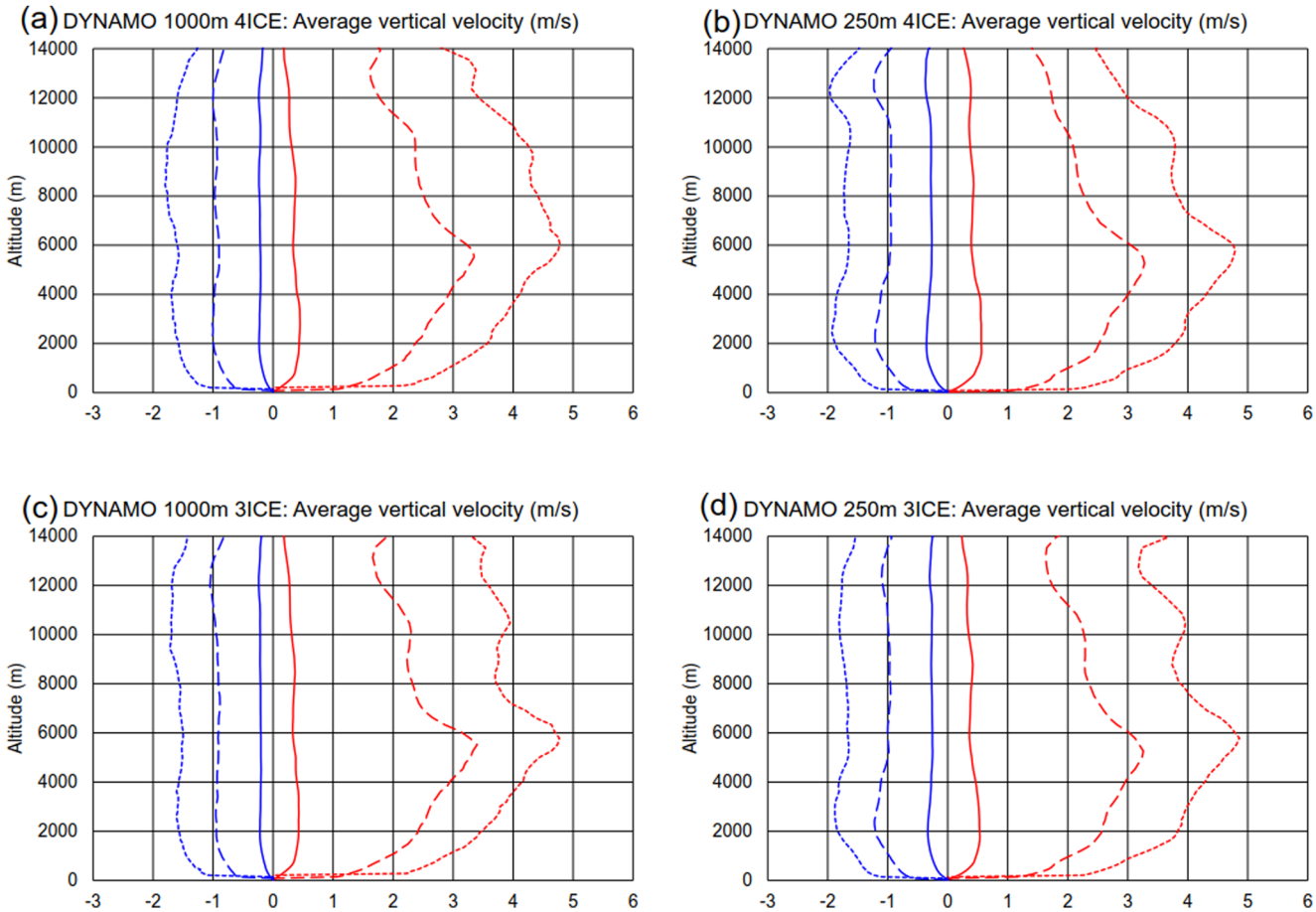

Figure 14. Vertical profiles of the mean upward (red lines) and downward (blue lines) vertical velocity inside of all clouds (solid lines) and inside the active updrafts and downdrafts for the four Dynamics of the Madden-Julian Oscillation (DYNAMO) simulations. The absolute vertical velocity exceeds 1 (long-dashed lines) or 2 (short-dash lines) m s^{-1} for active updrafts and 0.5 (long-dashed lines) and 1 (short-dashed lines) m s^{-1} for active downdrafts. Panel (a) shows the D4ICE, (b) the D4ICEH, (c) the D3ICE, and (d) the D3ICEH results.

Figure 14 shows the mean vertical velocities in the cloudy, active updraft and active downdraft regions for all four DYNAMO simulations. They all show that the mean upward and downward vertical velocity is less than 0.6 m s^{-1} for the cloudy region. Active updrafts are about 2–3 and 3–5 m s^{-1} for the 1 and 2 m s^{-1} thresholds, respectively. The active downdrafts are about 1 and 1–2 m s^{-1} for the absolute vertical velocity 0.5 and 1 m s^{-1} thresholds, respectively. All of the runs show that there are large mean updrafts (~4.5 m s^{-1}) located near the 6-km level. One difference is that the intensity of the cloudy (mean), active downdraft and updraft regions at low levels (~2 km) is slightly stronger in the high-resolution simulations (Figures 14b and 14d). The small difference is caused by the fact that identical forcing is imposed in these simulations.

Zipser and LeMone (1980) and Jorgensen and LeMone (1989) found that the intensity of active updrafts is about 2–3 m s^{-1} and active downdrafts about 2 m s^{-1} for GATE and a TAMEX squall case. The DYNAMO modeling results are in very good agreement with those observations. Note that the present model analysis is based on the mean (not median) updrafts and downdrafts. Another difference is that our analyses consider the whole model domain area, not the drafts and cores as in LeMone and Zipser. The GOAmozon modeling results are not in good agreement with Wang et al. (2019, 2022) at upper levels (10 km).

The shapes of the average updraft and downdraft velocity profiles differ. That is, the average vertical velocity profiles are nearly constant with height. The active downdrafts for both thresholds are likewise nearly constant with height, consistent with those reported in LeMone and Zipser (1980) and Jorgensen and LeMone (1989). On the other hand, the average vertical velocity profile for active updrafts of both thresholds has a maximum near

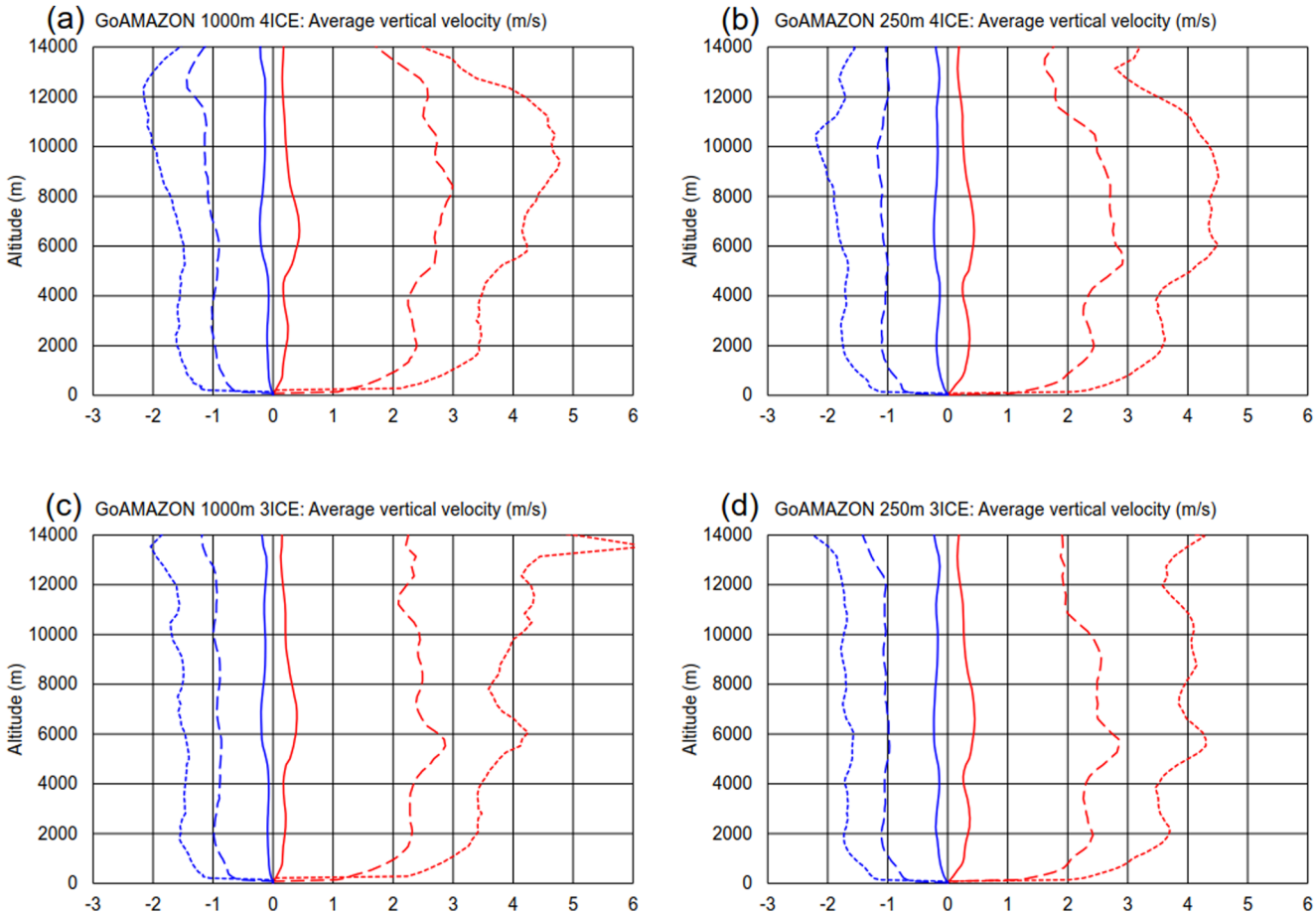

Figure 15. Same as Figure 14 except for the Green Ocean Amazon Experiment (GOAmazon) case.

6 km. No such maximum was detected in the aircraft measurements of Zipser and LeMone, but their measurements did not extend above 8 km.

Mean vertical velocities in cloudy active updraft and downdraft regions for all four GOAmazon simulations are also quite similar to each other (Figure 15). Active drafts are about 2–5 m s^{-1} for updrafts and 1–2 m s^{-1} for downdrafts. A linear uniform distribution for active downdrafts (at both the 0.5 or 1 m s^{-1} thresholds) is also evident in all four GOAmazon simulations from low-levels up to the 12-km level. The active updrafts are also quite similar in all four GOAmazon runs. They all increase from the surface up to the 6-km level. However, these active updrafts show some differences in the upper troposphere (above the 10-km level). One 3ICE run (G3ICE, Figure 15c) simulates stronger upward motion (>5–6 m s^{-1}) near the 14-km level with a 2 m s^{-1} threshold. The area coverage is very small in the upper troposphere—see Figure 13b, so sampling could be the reason for the difference. The distribution of active updrafts is somewhat similar to radar profiler as was the case for DYNAMO observations associated with mature MCSs (Wang et al., 2019, 2020). The observed distribution also shows an increase from the surface up to 6 km with the active updrafts continuing to intensify above the 6-km level. One major difference is that the observed active updrafts are stronger than the simulated. This could be due to the observations being for mature MCS types.

The vertical distribution and domain-time vertically integrated LH with respect to the total (cloudy) and active drafts for the DYNAMO case are shown in Figure 16 and Table 3, respectively. The percentage of each LH production rate in active updrafts and downdrafts with respect to the total LH production rate is also shown in Table 3. Almost all condensation (99%), deposition (96%), and freezing (95%) occurs in the updraft regions. On the other hand, more than 84% of evaporation and sublimation occur in the downdraft regions. There is more melting in the updraft (65%) region than the downdraft (35%) regions. Note that the melting in the updraft region

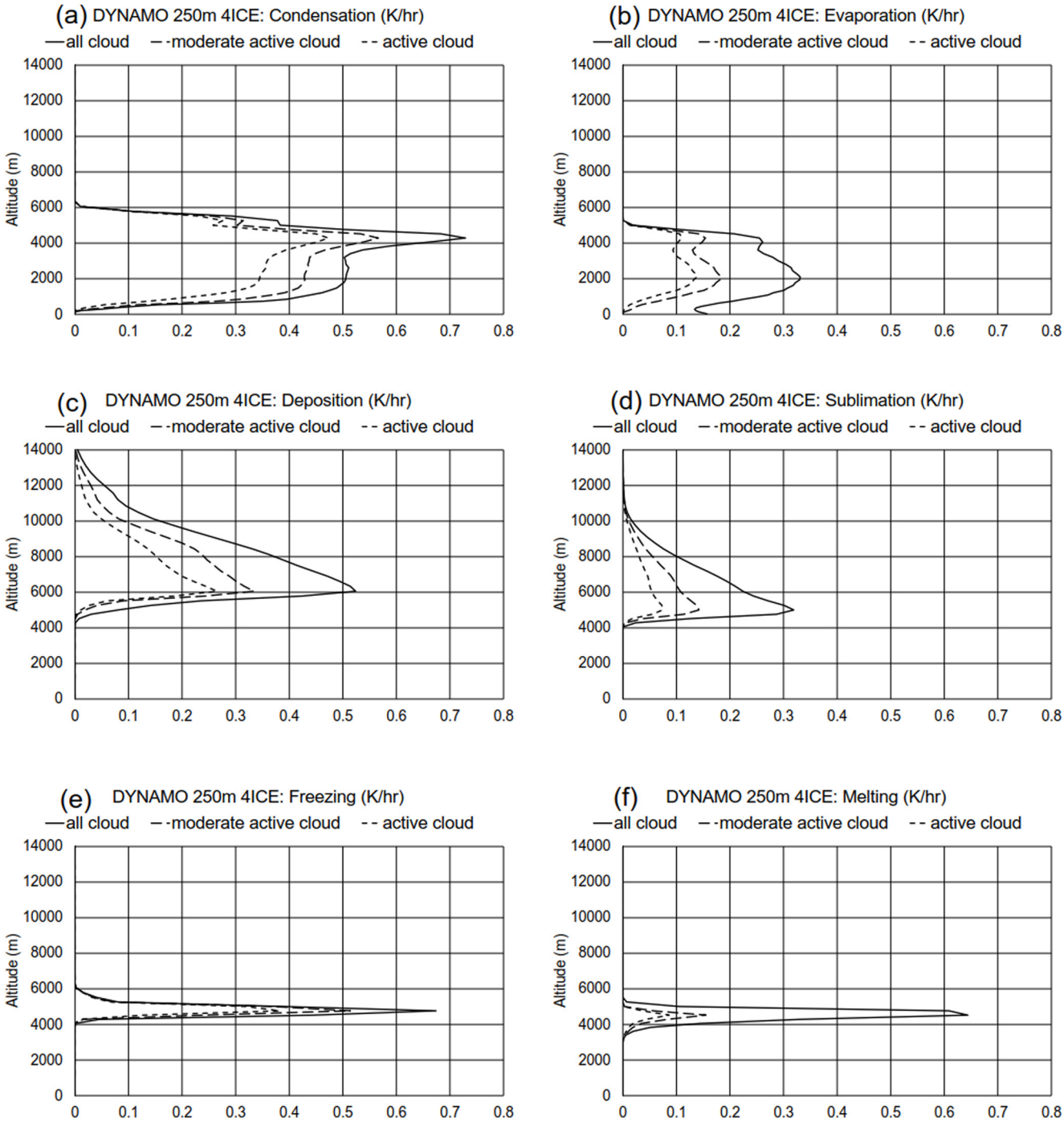

Figure 16. Vertical profiles of mean latent heating production rate due to the phase changes of water within cloud and active updraft and downdraft areas for the Dynamics of the Madden-Julian Oscillation (DYNAMO) case. Panel (a) shows condensation, (b) evaporation, (c) deposition, (d) sublimation, (e) freezing, and (f) meeting. Solid line is for all cloud, long-dashed line is for moderate active cloud ($w > 1$ m s^{-1} for condensation, deposition, and freezing, and $w < -0.5$ m s^{-1} for evaporation, sublimation, and melting) and short-dashed line is active cloud ($w > 2$ m s^{-1} and < -1 m s^{-1}).

is because the hail fall speeds allow hail to fall into the melting region even in updraft regions. Active updrafts with vertical velocities exceeding 1 and 2 m s^{-1} account for more than 80% and 65% of condensation, respectively (Figures 16a and 16f, Table 3). But, active downdrafts with vertical velocities exceeding |0.5| and |1| m s^{-1} account for less than 50% and 35% of the evaporation, respectively (Figure 16b, Table 3). Less evaporation than condensation occurs in inactive cloud regions (areas with vertical velocities less than |1| m s^{-1}). The contribution

Table 3
Domain and Time Averaged Vertically Integrated Latent Heating (LH) Change Rates (W m^{-2}) for the Whole Domain, Updraft and Downdraft Regions in the DYNAMO 4ICE Simulation With 250 m Model Resolution

	Condensation	Evaporation	Deposition	Sublimation	Melting	Freezing
Total	6.25E-04	3.22E-04	3.88E-04	2.37E-04	1.03E-04	9.02E-05
Updraft	99%	16%	96%	9%	65%	95%
$w > 1$ ms^{-1}	83%	1%	46%	<0.5%	43%	75%
$w > 2$ ms^{-1}	66%	<0.01%	32%	<0.1%	29%	58%
Downdraft	<1%	84%	4%	90%	35%	5%
$w < -0.5$ ms^{-1}	<0.01%	48%	<0.001%	44%	17%	3%
$w < -1$ ms^{-1}	<0.001%	33%	<0.0001%	24%	9%	1%

Note. The values for the updraft and downdraft regions are percentages of the total amounts. The LH rate in the inactive regions can be estimated from the difference between the total and active regions.

of sublimation in the active downdrafts (Figuer 16d, Table 3) is quite similar to that for evaporation. Active downdrafts exceeding |1| m s^{-1} only account for 24% of the sublimation. Active updrafts exceeding vertical velocities of 1 and 2 m s^{-1} account for more than 40% and 30% of deposition (Figure 16c) and melting (Figure 16e), respectively. This suggests that less deposition than condensation occurs in inactive cloud regions (areas with vertical velocities less than |1| m s^{-1}). The melting process also mainly occurs in the inactive downdraft region (Figure 16e). Note that these active updrafts and downdrafts only have small areal coverages (~2%) (Figure 13).

For the GOAmazon case, more than 95% of condensation, deposition and freezing occurs in the updraft regions while more than 85% of evaporation and sublimation occurs in the downdraft regions (Table 4). Overall, the contribution of active updrafts to condensation, evaporation, deposition and sublimation for the GOAmazon case is similar to that for DYNAMO. Active updrafts with vertical velocities exceeding 1 and 2 m s^{-1} account for more than 70% and 50% of condensation, respectively (Figure 17a, Table 4). Active downdrafts with vertical velocities exceeding |0.5| and |1| m s^{-1} account for less than 50% and 30% of the total evaporation, respectively (Figure 17b). Active updrafts exceeding a vertical velocity of 1 m s^{-1} account for more than 50% of deposition while active downdrafts exceeding |1| m s^{-1} only account for 23% of the sublimation (Figures 17c and 17d). Less condensation and freezing occur in the active drafts (Tables 3 and 4) compared to in DYNAMO, but sublimation in the active downdraft region and melting in the active updraft region are similar to DYNAMO. Some differences are caused by the difference in the areal coverage of active updrafts and downdrafts between the DYNAMO and GOAmazon cases.

Figure 18 shows the vertical distributions of the cloud hydrometeors in the cloud and active cloud draft (both upward and downward) regions for the DYNAMO case. All the types of hydrometeors exist in active updrafts and downdrafts. There is more cloud water in the active updraft region than in the active downdraft region (Figure 18a). Active updrafts with vertical velocities exceeding 1 m s^{-1} account for ~50% of the total cloud water. Cloud water in both the active and inactive cloudy region exhibits a sharp peak slightly above the 4-km level (near the freezing level) where there are also peaks in the condensation rate (Figure 16a). Rain mainly occurs in

Table 4
Same as Table 3 Except for the GOAmazon Case

W/m2	Condensation	Evaporation	Deposition	Sublimation	Melting	Freezing
Total	4.57E-04	2.12E-04	1.52E-04	9.48E-05	6.54E-05	6.48E-05
Updraft	99%	11%	97%	9%	77%	96%
$w > 1$ ms^{-1}	72%	<0.5%	52%	<0.5%	42%	62%
$w > 2$ ms^{-1}	51%	<0.1%	35%	<0.01%	23%	36%
Downdraft	1%	89%	3%	93%	23%	4%
$w < -0.5$ ms^{-1}	<0.01%	49%	<0.1%	43%	10%	2%
$w < -1$ ms^{-1}	<0.001%	31%	<0.01%	23%	5%	1%

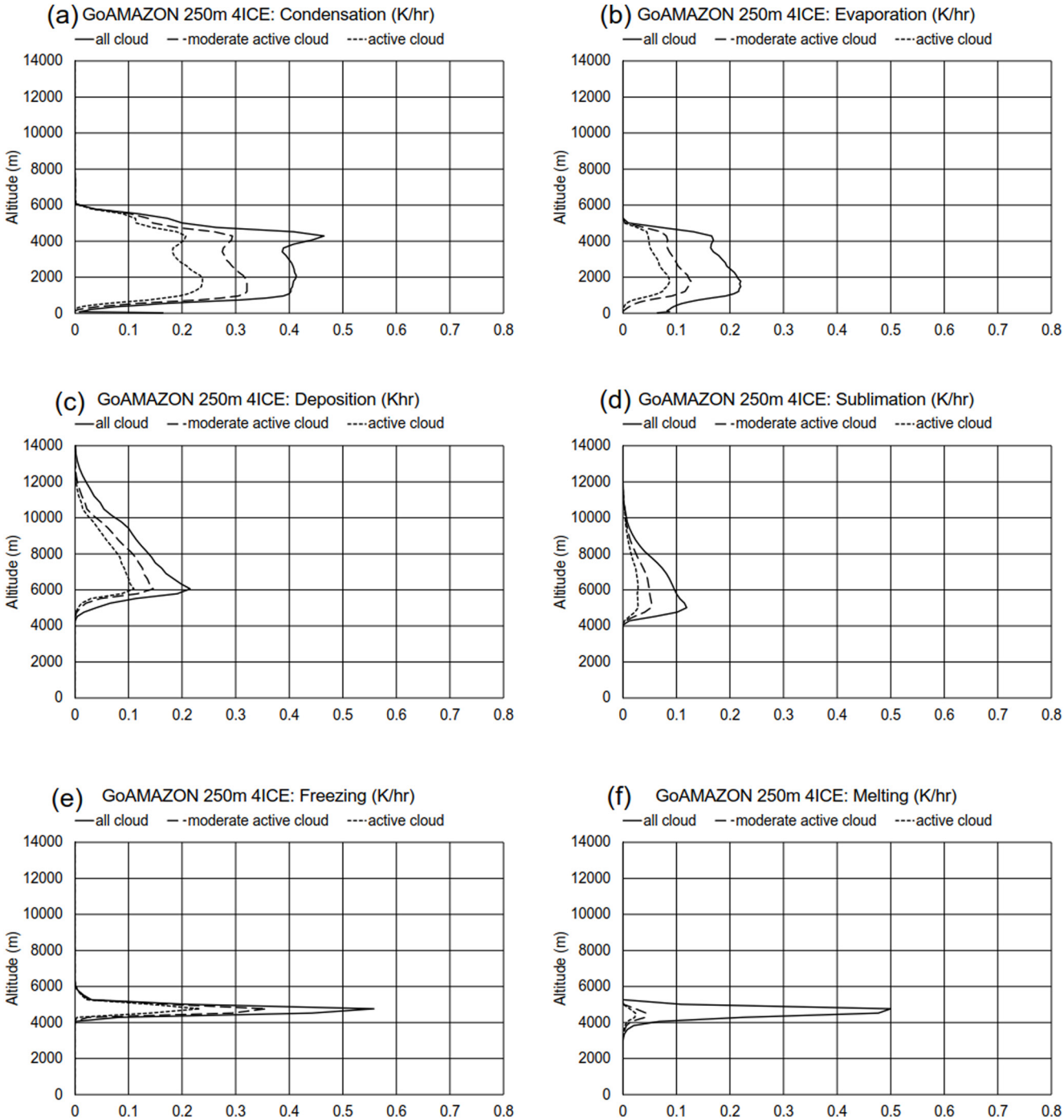

Figure 17. Same as Figure 16 except for the Green Ocean Amazon Experiment (GOAmazon) case.

the inactive cloudy (vertical velocity does not exceed |1| m s^{-1}) region (Figure 18b). More cloud ice, graupel, and hail mass occurs in the active updrafts than their counterparts in the active downdrafts (Figures 18c, 18e and 18f). Cloud ice and snow are mainly in the inactive cloud region (Figures 18c and 18d). Hail occurs primarily in the active updrafts (Figure 18f). Snow amounts are the largest while graupel and hail mass amounts are the least amount of precipitating ice. Graupel and hail amounts are one-order of magnitude smaller than for other cloud hydrometeors. They both have a sharp peak around the freezing level where there is a sharp peak in melting and freezing (Figures 16e and 16f). Note that there are little reports about the presence of hail being observed over tropical oceans.

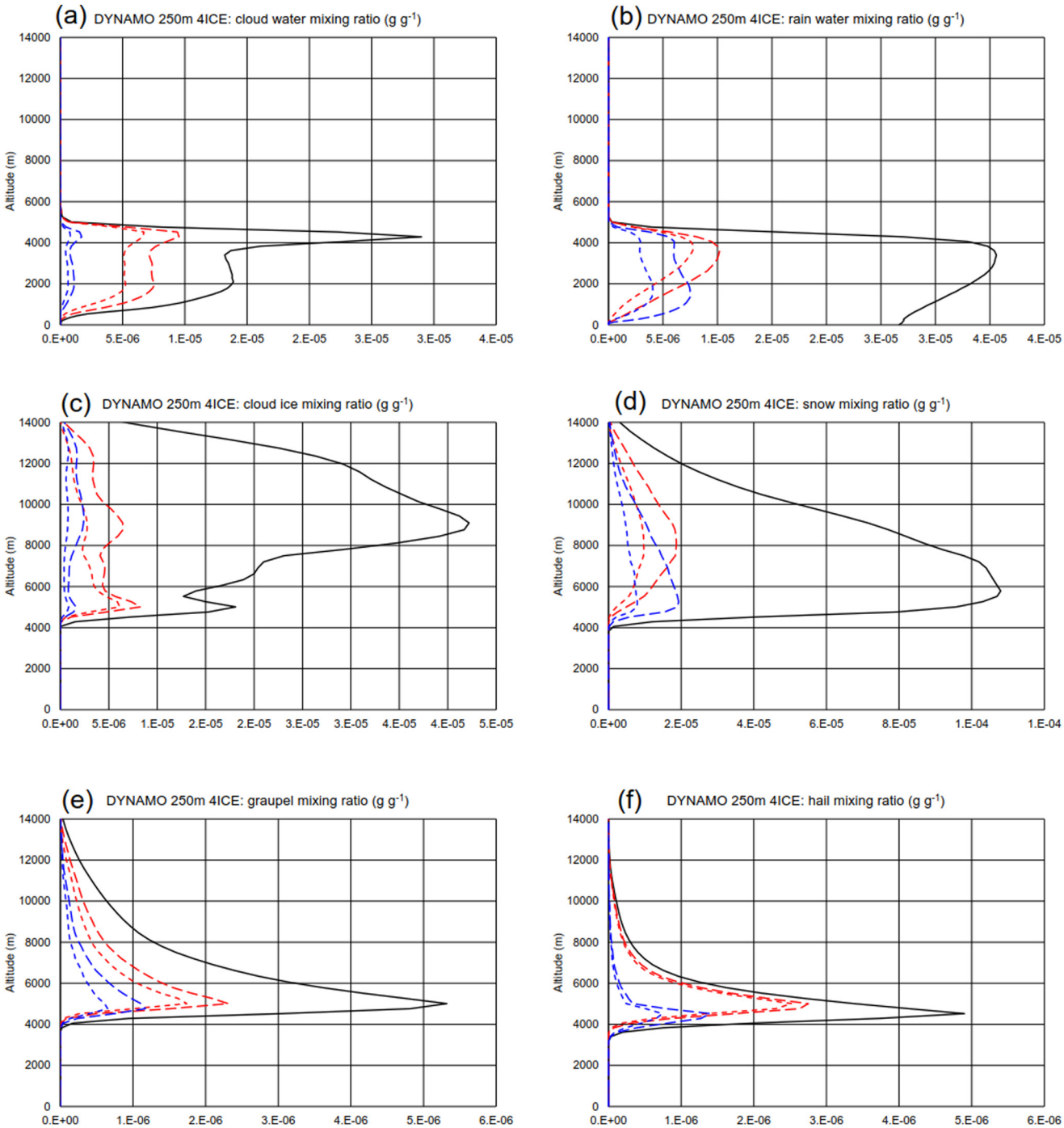

Figure 18. Vertical mean hydrometeor profiles within cloud and active updraft (red lines) and downdraft (blue lines) areas for the Dynamics of the Madden-Julian Oscillation (DYNAMO) case. Panel (a) shows cloud water, (b) rain, (c) cloud ice, (d) snow, (e) graupel, and (f) hail. Solid lines are for all cloud, long-dashed lines for active updrafts ($w > 2$ m s^{-1}), and short-dashed lines for moderately active updrafts ($w > 1$ m s^{-1}). For active downdrafts, long-dashed and short-dashed lines are for $|w| > 0.5$ and 1 m s^{-1}, respectively. Note that the horizontal scales are not the same for each panel. There are no reports about the presence of hail being observed over tropical oceans.

The vertical profiles of cloud hydrometeors in inactive and active cloud regions for the GOAmazon case are similar to those for the DYNAMO case. Rain, cloud ice and snow amounts in the active updraft and downdraft regions are much less than those in the inactive region (Figures 19a–19d). More hail and graupel can be found in the active updraft region than in the active downdraft region (Figures 19e and 19f). Their values are also quite

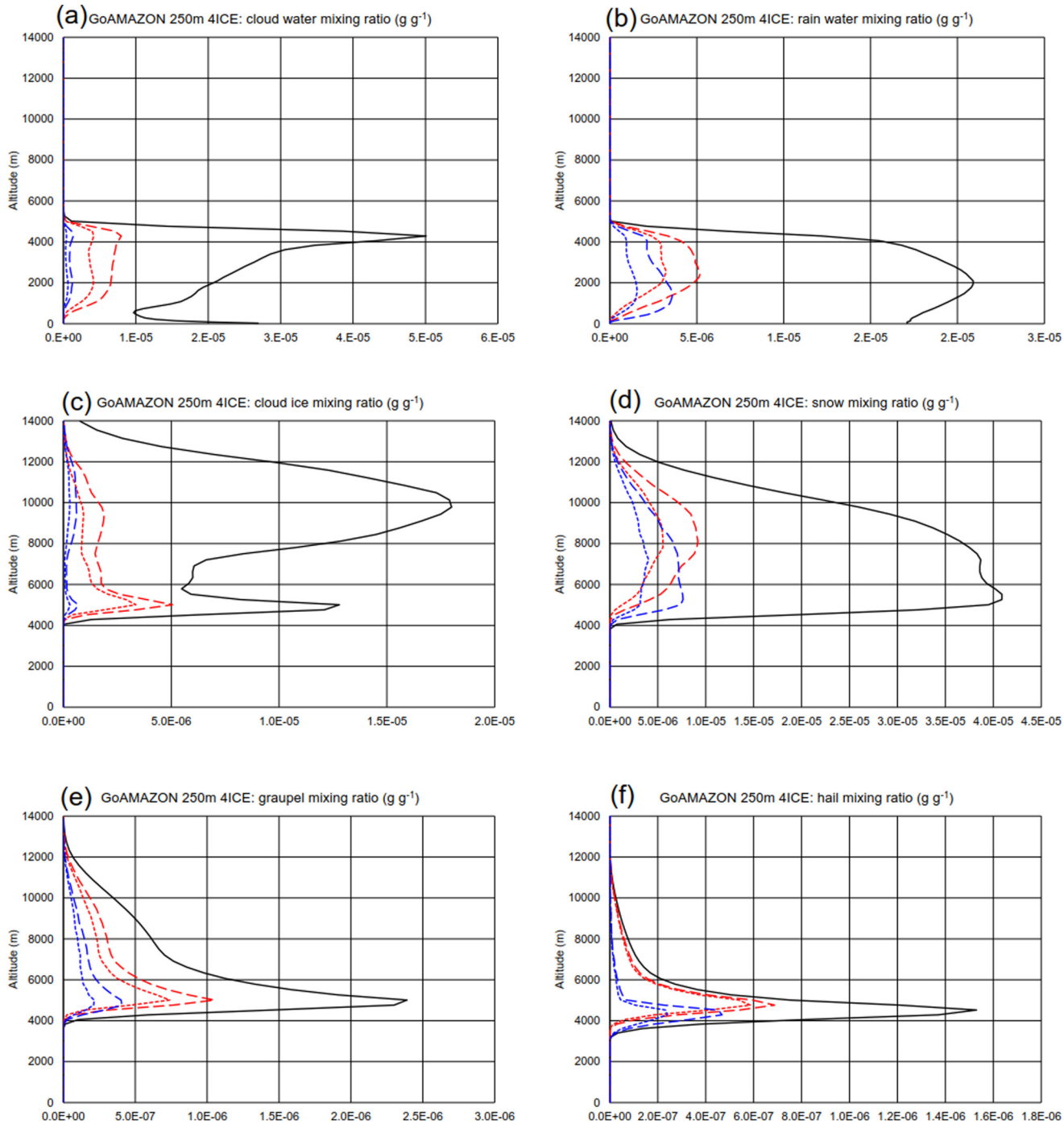

Figure 19. Same as Figure 18 except for the Green Ocean Amazon Experiment (GOAmazon) case.

small compared to other cloud hydrometeors. All of these results are in reasonable agreement with the DYNAMO case. However, the contribution of active updrafts for cloud water and hail are less than that in the DYNAMO case. In addition, there are two other major differences between the DYNAMO and GOAmazon cases. The first is that there is quite a large amount of cloud water near the surface in the GOAmazon case, and the second is that there is also quite a large amount of cloud ice near the 5-km level. An additional test was conducted to examine the impact of surface fluxes on the development of cloud water at and near the ground (surface). The results

show that there is no cloud water near the ground without the surface fluxes. The result indicates that surface fluxes are responsible for the cloud water at the model bottom.

4.5. Sensitivity to Microphysics and Model Resolution (Grid Spacing)

The model domain and time integrated mean LH terms (Figure 20) and hydrometeor contents (Figure 21) in the total region are used to assess the impact of different model grid spacings (250 vs. 1,000 m) and microphysics (3ICE vs. 4ICE) for both DYNAMO and GOAmazon. The results show that condensation is the largest term, while evaporation and deposition are the second largest LH terms for all four DYNAMO simulations (Figure 20a). Freezing and melting are the smallest contributors to LH (Figure 20a). All of these LH contribution characteristics are also evident in the four GOAmazon simulations (Figure 20b). One difference between the DYNAMO and GOAmazon cases is that all of the LH terms are greater in DYNAMO. In addition, deposition (sublimation) is only 25% of condensation (evaporation) in the GOAmazon case. In contrast, deposition (sublimation) is about 50% of condensation (evaporation) for the DYNAMO case. This suggests warm rain processes are more dominant in the GOAmazon case than in DYNAMO. In addition, the model grid spacing and microphysics do not have a noted impact on the time and domain integrated surface precipitation (Table 2) and abovementioned LH quantities.

Figure 21 shows that snow is the largest hydrometeor mass in the total, while rain is the second largest hydrometeor overall in all four DYNAMO simulations. Graupel and hail have the smallest amounts in the total region. Cloud water and rain amounts are similar to or exceed snow in the total region, respectively, for the GOAmazon case. Note that a log scale is used in Figure 21. Consequently, the total snow, rain, cloud water and cloud ice contents are much larger than those of graupel and hail for both DYNAMO and GOAmazon. Also, the difference in hail content is much smaller than the differences in cloud water, rain, cloud ice and snow in both DYNAMO and GOAmazon.

4.5.1. Impact of Model Resolution (or Grid Spacing)

The high-resolution simulations have more condensation, evaporation, deposition, sublimation and melting in the total than those using coarser resolution for both the 3ICE (red vs. yellow in Figure 20) and 4ICE (blue vs. light blue in Figure 20) schemes, as well as for both the DYNAMO and GOAmazon cases. Freezing is also larger with higher resolution (G3ICEH and G4ICE4 vs. G3ICE and G4ICE) in the total for GOAmazon. The difference in freezing between D3ICE and D3ICEH and between D4ICE and D4ICEH is quite small in the total regions. Evaporation and sublimation in the stratiform region are larger in D3ICEH and D4ICEH than in D3ICE and D4ICE, respectively.

The results show there is little difference in the total rain and snow between D4ICEH and D4ICE or between D3ICEH and D3ICE in the total (blue vs. light blue in Figure 21a). More hail is simulated in D4ICEH than D4ICE cases. D4ICEH (D3ICEH) has slightly less cloud water than D4ICE (D3ICE). A major difference between the high and low-resolution runs using the 3ICE scheme is that D3ICEH has more graupel than D3ICE (yellow and red in Figure 21). There are greater differences in the hydrometeor amounts between D3ICEH and D3ICE than between D4ICEH and D4ICE.

For GOAmazon, G4ICEH has less cloud water and slightly more cloud ice than G4ICE for the total regions (blue and light blue in Figure 21b). Rainwater, snow, graupel, and hail show small differences between G4ICEH and G4ICE cases. For the 3ICE scheme, G3ICEH has less cloud water and more graupel than G3ICE in the total (red and yellow in Figure 21a). Differences in rain and snow are small between these two cases.

4.5.2. Impact by Microphysical Schemes

The D4ICEH case has slightly more total condensation and evaporation but less deposition, sublimation, melting and freezing than D3ICEH (blue vs. red color in Figure 20a). D4ICE has more condensation and evaporation but less melting and freezing compared to D3ICE (yellow and light blue in Figure 20a). For DYNAMO, the 4ICE scheme generally has more condensation and evaporation but less melting and freezing than the 3ICE scheme. However, this sensitivity is less than when using different model grid spacings (1,000 and 250 m).

For GOAmazon, the microphysical rate differences between G4ICE and G3ICE are generally quite small in the total regions (light blue vs. yellow in Figure 20b). However, there are differences. G4ICE has more condensation

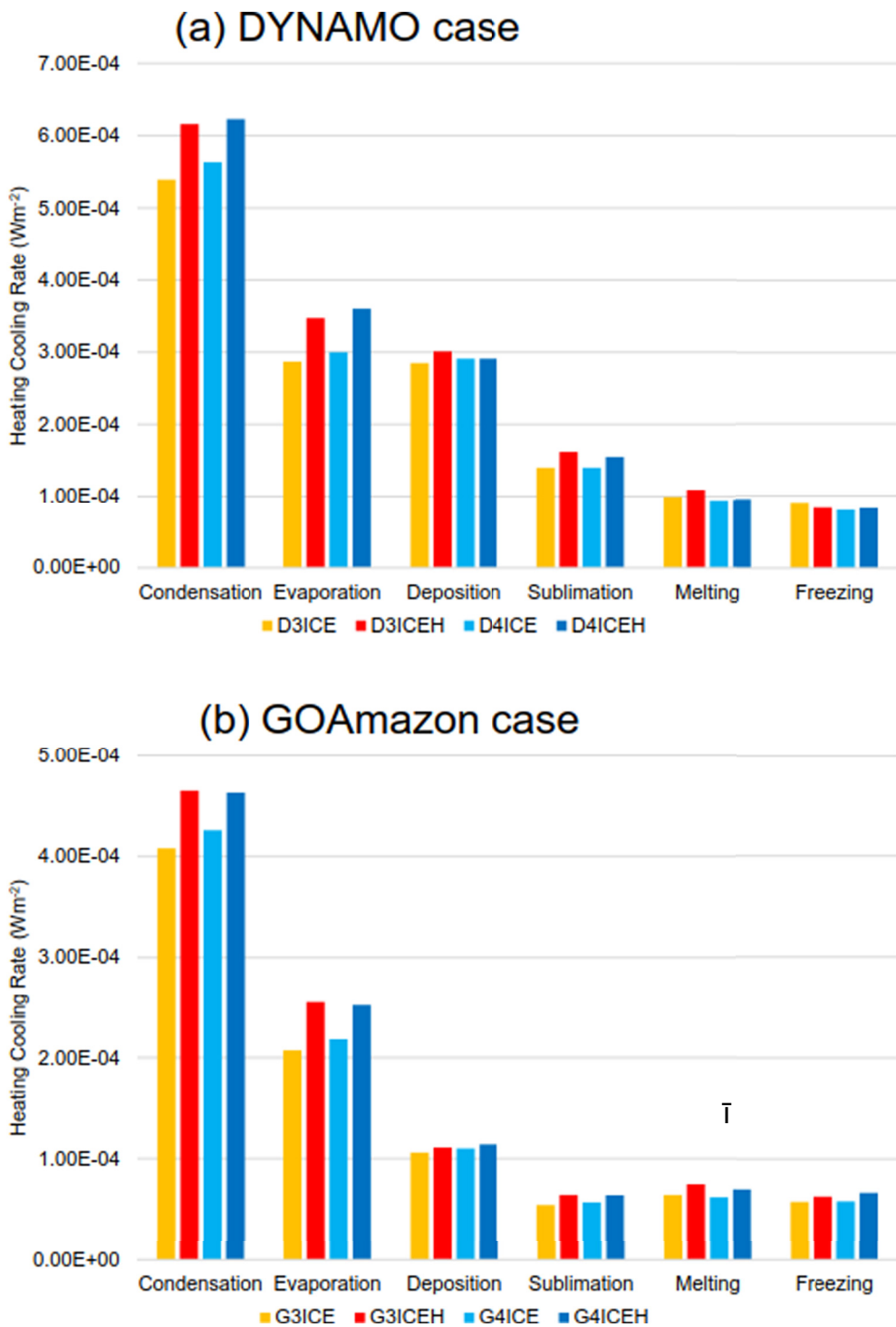

Figure 20. Domain and time (15 days) averaged, vertically integrated latent heating production rates (condensation, evaporation, deposition, sublimation, freezing, and melting) for the (a) Dynamics of the Madden-Julian Oscillation (DYNAMO) and (b) Green Ocean Amazon Experiment (GOAmazon) cases, respectively. Note that the scale (rate) is different between the DYNAMO and GOAmazon cases.

and evaporation than G3ICE case (light blue vs. yellow in Figure 20b). For, GOAmazon, the largest microphysics sensitivity is with warm rain processes at coarser model resolution. Model resolution has a greater impact on the integrated LH terms than the microphysics parameterization for both the DYNAMO and GOAmazon cases.

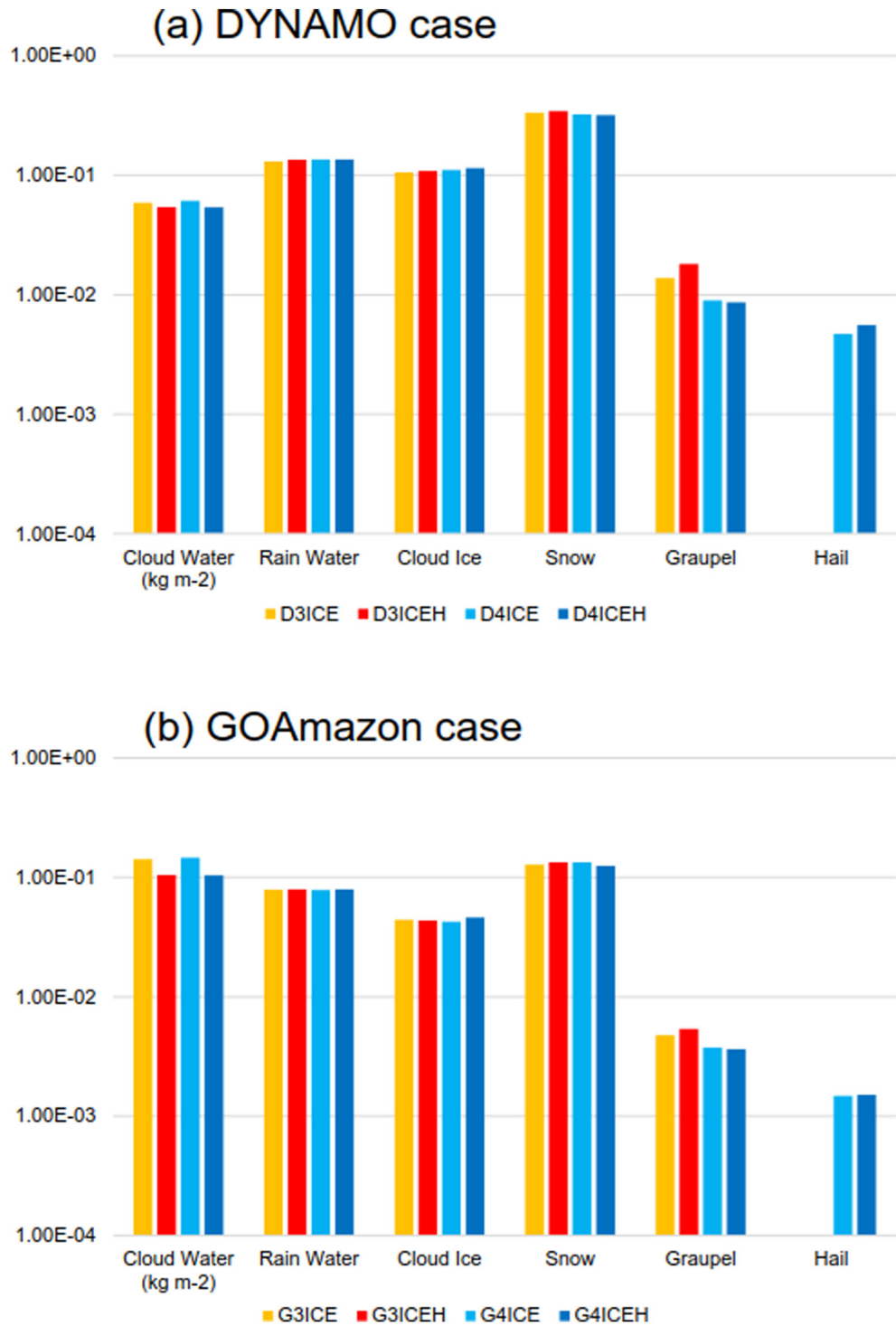

Figure 21. Same as Figure 20 except for total hydrometeors (cloud water, rain, cloud ice, snow, graupel, and hail). Note that the log scale is used.

A major difference between the different microphysics schemes is the graupel amount for both the DYNAMO and GOAmazon cases. There is more graupel in D3ICEH and G3ICEH than in D4ICEH and G4ICEH, respectively (blue vs. red in Figure 21). This difference is also evident at low-resolution (D3ICE vs. D4ICE and G3ICE vs. G4ICE; light blue vs. yellow in Figure 21).

Neither model grid-spacing nor microphysics has much impact on the amount of rainwater for either GOAmazon or DYNAMO; the total surface rainfall amounts are quite similar in all four DYNAMO and all four GOAmazon simulations (Table 2). This is because increased condensation is balanced by increased evaporation (Figure 20). Consequently, the net condensation is similar in all four DYNAMO and all four GOAmazon simulations, respectively. Similar balance also occurs between the net deposition and sublimation for all simulations.

5. Summary

Fifteen-day 2D GCE model simulations for two tropical cases (DYNAMO and GOAmazon) were conducted to examine the relationship between LH processes and cloud properties (hydrometeors) with respect to vertical velocity. The model simulated a population of different types of clouds and convective systems over their respective life cycles in both cases. The simulated LH processes and cloud properties were then separated into convective and stratiform regions, as well as active and inactive cloud regimes. Sensitivity tests were also performed to examine the impact of model resolution (i.e., 250- and 1,000-m grid spacing) and microphysics scheme (3 classes of ice with cloud ice, snow, and graupel and 4 classes of ice with cloud ice, snow, graupel, and hail) on the model simulated LH and cloud properties. The major findings are as follows:

- GCE-simulated condensation, deposition and freezing occur mainly in moderate to strong updrafts, peak evaporation and sublimation occur predominantly in weak (1–2 m s^{-1}) and moderate downdrafts regions, while melting occurs in moderate to strong updrafts and downdrafts in the convection regions for both the DYNAMO and GOAmazon case. GCE-simulated evaporation, sublimation, freezing and melting occur mainly in weak to moderate downdraft regions in the stratiform regions. The freezing in this downdraft regions only occurs if liquid hydrometeors are falling at altitudes where ambient temperatures are below 0°C. One difference between the two cases is that cloud water and rain occur over a narrower range of drafts while cloud ice, snow, graupel, and hail extend over a greater range of stronger updrafts and downdrafts in GOAmazon. Another difference is condensation, evaporation, freezing and melting are slightly weaker in the GOAmazon case.
- GCE-simulated fractional areal coverage of active updrafts with vertical velocities exceeding 1 and 2 m s^{-1} is only about 1.2% and 0.5% of the total domain, respectively, for the DYNAMO case. LeMone and Zipser (1980) also found only a small percentage of areal coverage by active drafts (a few percent) over the area sampled by aircraft. For the GOAmazon case, the fractional area coverage of active cloud drafts is even less compared with observations and DYNAMO. This result suggests that although active updrafts cover only a small area (a few percent) of the model domain, they contribute significantly to the latent heat release and are associated with large proportions of the hydrometeors.
- GCE-simulated active updrafts with vertical velocities greater than 1 m s^{-1} account for more than 75% and 70% of the condensation respectively, for the DYNAMO and GOAmazon case. However, the active downdrafts with vertical velocities exceeding |1| m s^{-1} account for less than 35% and 30% of the evaporation and sublimation, respectively for the DYNAMO and GOAmazom case. There is greater evaporation and sublimation than condensation in inactive cloud regions for both cases. Melting largely occurs in the active updraft and inactive downdraft cloud area for both cases. However, there is greater deposition and less melting and freezing in the active drafts in GOAmazon compared to DYNAMO. Some of the differences are caused by the difference in areal coverage of active updrafts and downdrafts between the DYNAMO and GOAmazon cases.
- GCE-simulated rain, cloud ice, snow, and graupel are mainly located in the inactive cloudy region for the DYNAMO case. About 50% of the cloud water and 70% of the hail are in active updrafts with vertical velocities greater than 2 m s^{-1} for the DYNAMO case. However, almost all of the hydrometeors are located in the inactive cloudy region for the GOAmazon case.
- GCE-simulated graupel is more in the 3ICE than in the 4ICE scheme. This is because the 4ICE scheme has an additional hail category. The differences in cloud water, rain, cloud ice, and snow between 3ICE and 4ICE scheme are generally quite small for both cases.
- GCE-simulated amounts of cloud water and cloud ice in the updraft region and their structures (shapes) are quite similar to the condensation and deposition, respectively. The simulated rain in the downdraft region has a similar structure to the evaporation rate. This result suggests that there is a relationship between LH release (heating) and smaller hydrometeors (cloud and water) and LH absorption (cooling) with larger hydrometeors (rain).

One of the primary ACCP goals is the improvement of cloud and precipitation processes in Earth system models (Gettelman et al., 2021) through the use of focused, global, space-borne *co-located* measurements of convective vertical velocities and cloud and precipitation mixing ratios. While our current Earth observing systems have provided us with unprecedented views of cloud structures, bulk microphysical properties, and precipitation, the complete absence, to date, of global Doppler measurements of convective vertical velocities has meant that (a) assessing the links between the dynamical and microphysical processes of convective systems has been extremely challenging, and (b) we have had to rely on CRMs to produce global LH products (e.g., Tao et al., 2010). As convective storm processes form one of the primary pillars of a potential ACCP program, critical observations and associated retrievals of storm-scale vertical motion, co-located dynamical and microphysical properties, precipitation characteristics, and LH will form the basis of the approach for enhancing our understanding of convective storm processes (see question W-4 from the 2017–2027 Decadal Survey, National Academies, 2018). The high-resolution modeling results described in this paper could provide a testbed for future orbital and suborbital elements of ACCP science, including facilitating observing system simulation experiments. The results could also provide a database to relate measured vertical velocity and associated hydrometeor structures.

There are limitations in the current study that could be improved with future studies. For example, only two tropical convective precipitation cases are simulated. Additional cases and different microphysical schemes may be required to generalize the results presented in this study. Limitations in microphysical schemes and imposed surface fluxes in the GOAmazon case have produced some discrepancies compared with the observations, such as hail (DYNAMO case) and fog (GOAmazon case) formation. These need to be confirmed and addressed in additional case studies. Cloud processes are 3D in nature, but it is still very computationally challenging to conduct high-resolution (i.e., 250 m) simulations with large domains (i.e., 1,024 km) for multi-day model integrations (i.e., 15 days). Please note that the simulation of deep moist convection requires O(100 m) grid spacing or better, and 250 m is right on the edge of what is acceptable (Bryan et al., 2003). In a subsequent paper, 3D simulations (with 500-m grid spacing with a relatively small domain, 512 × 128 grid points) will be presented and additional statistical analysis for cloud and microphysical processes (i.e., conversion processes from different hydrometeors) will be conducted.

Data Availability Statement

The large-scale forcing for Green Ocean Amazon Experiment and Dynamics of the Madden-Julian Oscillation was provided by Dr. Shaocheng Xie and Shuaiqi Tang at the DOE Livermore National Laboratory (https://iop.archive.arm.gov/arm-iop/0eval-data/xie/scm-forcing/iop_at_mao/GOAMAZON/?ticket=ST-79804-k0h8p-BOeLdd-WkVElNn9J73XpVQsso and https://iop.archive.arm.gov/arm-iop/0eval-data/xie/scm-forcing/iop_at_gan/). Model data used in this study are available from the Goddard Mesoscale Modeling and Dynamics Group's Cloud Library data portal https://portal.nccs.nasa.gov/cloudlibrary-data//PUB_DATA/JAMES_2021_Tao/.

Acknowledgments
This research was supported by the NASA Precipitation Measuring Mission (PMM, grant numbers 573945.04.80.01.04 and 80NSSC19K0738) and NASA Modeling, Analysis and Prediction (MAP, grant number 509496.02.08.10.06). The authors are grateful to Dr. G. Skofronick-Jackson and Dr. David Considine at NASA headquarters for their support of this research. Acknowledgment is also made to the NASA Goddard Space Flight Center and NASA Ames computing centers for the computational resources used in this research. The authors also thank three anonymous reviewers for their helpful comments, which helped to improve this paper.

References

Alexaner, G. D., & Cotton, W. R. (1998). The use of cloud-resolving simulations of mesoscale convective systems to build a meso-scale parameterization scheme. *Journal of the Atmospheric Sciences*, *55*(12), 2137–2161. https://doi.org/10.1175/1520-0469(1998)055<2137:TUOCRS>2.0.CO;2

Bryan, G. H., Wyngaard, J. C., & Fritsch, J. M. (2003). Resolution requirements for the simulation of deep moist convection. *Monthly Weather Review*, *131*(10), 2394–2416. https://doi.org/10.1175/1520-0493(2003)131<2394:rrftso>2.0.co;2

Chern, J.-D., Tao, W.-K., Lang, S. E., Li, J.-L. F., Mohr, K. I., Skofronick-Jackson, G. M., et al. (2016). Performance of the Goddard Multi-scale modeling framework with Goddard microphysical schemes. *Journal of Advances in Modeling Earth Systems*, *8*(1), 66–95. https://doi.org/10.1002/2015MS000469

Chern, J.-D., Tao, W.-K., Lang, S. E., Li, X., & Matsui, T. (2020). Evaluation precipitation features and rainfall characteristics in a multi-scale modeling framework. *Journal of Advances in Modeling Earth Systems*, *12*(8), e2019MS002007. https://doi.org/10.1029/2019MS002007

Chin, H.-N. S. (1994). The impact of the ice phase and radiation on a midlatitude squall line system. *Journal of the Atmospheric Sciences*, *51*(22), 3320–3343. https://doi.org/10.1175/1520-0469(1994)051<3320:TIOTIP>2.0.CO;2

Chou, M.-D., Lee, K.-T., Tsay, S.-C., & Fu, Q. (1999). Parameterization for cloud longwave scattering for use in atmospheric models. *Journal of Climate*, *12*(1), 159–169. https://doi.org/10.1175/1520-0442(1999)012<0159:PFCLSF>2.0.CO;2

Chou, M.-D., & Suarez, M. J. (1999). A solar radiation parameterization for atmospheric studies (NASA Tech. Rep. NASA/TM-1999-10460, Vol. *15*, p. 38).

Ciesielski, P. E., Johnson, R. H., Tang, S., Zhang, Y., & Xie, S. (2021). Comparison of conventional and constrained variational methods for computing large-scale budgets and forcing fields. *Journal of Geophysical Research: Atmospheres*, *126*(16), e2021JD035183. https://doi.org/10.1029/2021JD035183

Gettelman, A., Carmichael, G. R., Feingold, G., da Silva, A. M., & van den Heever, S. C. (2021). Confronting future models with future Satellite observations of clouds and aerosols. *Bulletin of the American Meteorological Society*, *102*(8), E1557–E1562. https://doi.org/10.1175/bams-d-21-0029.1

Giangrande, S. E., Toto, T., Jensen, M. P., Bartholomew, M. J., Feng, Z., Protat, A., et al. (2016). Convective cloud vertical velocity and mass-flux characteristics from radar wind profiler observations during GOAmazon2014/5. *Journal of Geophysical Research: Atmosphere*, *121*(21), 12891–12913. https://doi.org/10.1002/2016JD025303

Grant, L. D., van den Heever, S. C., Haddad, Z. S., Bukowki, J., Marinescu, P. J., Storer, R. L., et al. (2022). A linear relationship between vertical velocity and microphysical process rates in deep convection. *Journal of the Atmospheric Sciences*, *79*(2), 449–466. https://doi.org/10.1175/JAS-D-21-0035.1

Heymsfield, G. M., Tian, L., Heymsfield, A. J., Li, L., & Guimond, S. (2010). Characteristics of deep tropical and subtropical convection from nadir-viewing high-altitude airborne Doppler radar. *Journal of the Atmospheric Sciences*, *67*(2), 285–308. https://doi.org/10.1175/2009JAS3132.1

Houze, R. A., Jr. (1982). Cloud clusters and large-scale vertical motions in the tropics. *Journal of the Meteorological Society of Japan*, *60*(1), 396–409. https://doi.org/10.2151/jmsj1965.60.1_396

Jensen, M. P., Petersen, W. A., Bansemer, A., Bharadwaj, N., Carey, L. D., Cecil, D. J., et al. (2016). The midlatitude continental convective cloud experiment (MC3E). *Bulletin of the American Meteorological Society*, *97*(9), 1667–1686. https://doi.org/10.1175/BAMS-D-14-00228.1

Johnson, R. H. (1984). Partitioning tropical heat and moisture budgets into cumulus and mesoscale components: Implication for cumulus parameterization. *Monthly Weather Review*, *112*(8), 1656–1665. https://doi.org/10.1175/1520-0493(1984)112<1590:PTHAMB>2.0.CO;2

Johnson, R. H., & Ciesielski, P. E. (2013). Structure and properties of Madden-Julian Oscillations deduced from DYNAMO sounding array. *Journal of the Atmospheric Sciences*, *70*(10), 3157–3179. https://doi.org/10.1175/JAS-D-13-065.1

Johnson, R. H., Ciesielski, P. E., Ruppert, J. H., Jr., & Katsumata, M. (2015). Sounding-based thermodynamic budgets for DYNAMO. *Journal of the Atmospheric Sciences*, *72*(2), 598–622. https://doi.org/10.1175/JAS-D-14-0202.1

Jorgensen, D. P., & LeMone, M. A. (1989). Vertical velocity characteristics of oceanic convection. *Journal of the Atmospheric Sciences*, *46*(5), 621–640. https://doi.org/10.1175/1520-0469(1989)046<0621:VVCOOC>2.0.CO;2

Klemp, J. B., & Wilhelmson, R. B. (1978). The simulation of three dimensional convective storm dynamics. *Journal of the Atmospheric Sciences*, *35*(6), 1070–1096. https://doi.org/10.1175/1520-0469(1978)035<1070:TSOTDC>2.0.CO;2

Lang, S., Tao, W.-K., Cifelli, R., Olson, W., Halverson, J., Rutledge, S., & Simpson, J. (2007). Improving simulations of convective system from TRMM LBA: Easterly and Westerly regimes. *Journal of the Atmospheric Sciences*, *64*(4), 1141–1164. https://doi.org/10.1175/JAS3879.1

Lang, S., Tao, W.-K., Simpson, J., & Ferrier, B. (2003). Modeling of convective-stratiform precipitation processes: Sensitivity to partitioning methods. *Journal of Applied Meteorology*, *42*(4), 505–527. https://doi.org/10.1175/1520-0450(2003)042<0505:MOCSPP>2.0.CO;2

Lang, S., Tao, W.-K., Zeng, X., & Li, Y. (2011). Reducing the biases in simulated radar reflectivities from a bulk microphysics scheme: Tropical convective systems. *Journal of the Atmospheric Sciences*, *68*(10), 2306–2320. https://doi.org/10.1175/JAS-D-10-05000.1

Lang, S. E., & Tao, W.-K. (2018). The next-generation Goddard convective-stratiform heating algorithm: New tropical and warm season retrievals for GPM. *Journal of Climate*, *31*(15), 5997–6026. https://doi.org/10.1175/JCLI-D-17-0224.1

Lang, S. E., Tao, W.-K., Chern, J.-D., Wu, D., & Li, X. (2014). Benefits of a fourth ice class in the simulated radar reflectivities of convective systems using a bulk microphysics scheme. *Journal of the Atmospheric Sciences*, *71*(10), 3583–3612. https://doi.org/10.1175/JAS-D-13-0330.1

LeMone, M. A., & Zipser, E. J. (1980). Cumulonimbus vertical velocity events in GATE. Part I: Diameter, intensity and mass flux. *Journal of the Atmospheric Sciences*, *37*(11), 2444–2457. https://doi.org/10.1175/1520-0469(1980)037<2444:CVVEIG>2.0.CO;2

Li, X., Janiga, M., Wang, S., Tao, W.-K., Rowe, A., Xu, W., et al. (2018). Precipitation structure evolution during November DYNAMO MJO event: Cloud-resolution simulations and comparison with multiple radar observations. *Journal of Geophysical Research: Atmosphere*, *123*(7), 3530–3555. https://doi.org/10.1002/2017JD027775

Li, X., Tao, W.-K., Khain, A., Simpson, J., & Johnson, D. (2009a). Sensitivity of a cloud-resolving model to bulk and explicit-bin microphysics schemes: Part I: Comparisons. *Journal of the Atmospheric Sciences*, *66*(1), 3–21. https://doi.org/10.1175/2008JAS2646.1

Li, X., Tao, W.-K., Khain, A., Simpson, J., & Johnson, D. (2009b). Sensitivity of a cloud-resolving model to bulk and explicit-bin microphysics schemes: Part II: Cloud microphysics and storm dynamics interactions. *Journal of the Atmospheric Sciences*, *66*(1), 22–40. https://doi.org/10.1175/2008JAS2647.1

Lin, X., & Johnson, R. H. (1996). Heating, moistening, and rainfall over the western Pacific during TOGA COARE. *Journal of the Atmospheric Sciences*, *53*(22), 3367–3383. https://doi.org/10.1175/1520-0469(1996)053,3367:HMAROT.2.0.CO;2

Martin, S. T., Artaxo, P., Machado, L. A. T., Manzi, A. Q., Souza, R. A. F., Schumacher, C., et al. (2016). Introduction: Observations and modeling of the Green Ocean Amazon (GOAmazon2014/5). *Atmospheric Chemistry and Physics*, *16*(8), 4785–4797. https://doi.org/10.5194/acp-16-4785-2016

Matsui, T., Chern, J., Tao, W.-K., Lang, S., Satoh, M., Hashino, T., & Kubota, T. (2016). Land-ocean contrast of tropical cloud-precipitation signals derived from the TRMM Satellite and global storm-resolving models. *Journal of Hydrometeorology*, *17*(5), 1425–1445. https://doi.org/10.1175/JHM-D-15-0111.1

Matsui, T., Dolan, B., Rutledge, S. A., Tao, W.-K., Iguchi, T., Barnum, J., & Lang, S. (2019). POLARRIS: APOLArimetric radar retrieval and instrument simulators. *Journal of Geophysical Research: Atmosphere*, *124*(8), 4634–4657. https://doi.org/10.1029/2018JD028317

National Academies. (2018). *Thriving on our changing planet: A decadal strategy for Earth observation from space* (p. 694). National Academies Press.

Redelsperger, J.-L., Brown, P. R. A., Guichard, F., How, C., Kawasima, M., Lang, S., et al. (2000). A GCSS model intercomparison for a tropical squall line observed during TOGA-COARE. Part I: Cloud-resolving models. *Quarterly Journal of the Royal Meteorological Society*, *126*(564), 823–863. https://doi.org/10.1002/qj.49712656404

Shige, S., Takayabu, Y. N., Kida, S., Tao, W.-K., Zeng, X., & L'Ecuyer, T. (2009). Spectral retrieval of latent heating profiles from TRMM PR data. Part IV: Comparisons of lookup tables from two- and three-dimensional simulations. *Journal of Climate*, *22*(20), 5577–5594. https://doi.org/10.1175/2009JCLI2919.1

Smolarkiewicz, P. K., & Grabowski, W. W. (1990). The multidimensional positive advection transport algorithm: Nonoscillatory option. *Journal of Computational Physics*, *86*(2), 355–375. https://doi.org/10.1016/0021-9991(90)90105-A

Soong, S.-T., & Ogura, Y. (1980). Response of tradewind cumuli to large-scale processes. *Journal of the Atmospheric Sciences*, *37*(9), 2035–2050. https://doi.org/10.1175/1520-0469(1980)037<2035:ROTCTL>2.0.CO;2

Soong, S.-T., & Tao, W.-K. (1980). Response of deep tropical clouds to mesoscale processes. *Journal of the Atmospheric Sciences*, *37*(9), 2016–2036. https://doi.org/10.1175/1520-0469(1980)037<2016:RODTCC>2.0.CO;2

Tang, S., Xie, S., Zhang, Y., Zhang, M., Schumacher, C., Upton, H., et al. (2016). Large-scale vertical velocity, diabatic heating and drying profiles associated with seasonal and diurnal variations of convective systems observed in the GOAmazon2014/5 experiment. *Atmospheric Chemistry and Physics*, *16*(22), 14249–14264. https://doi.org/10.5194/acp-16-14249-2016

Tao, W.-K., & Chern, J. (2017). The impact of mesoscale convective systems on global precipitation: A modeling study. *Journal of Advances in Modeling Earth Systems*, *9*(2), 790–809. https://doi.org/10.1002/2016MS000836

Tao, W.-K., Lang, S., Zeng, X., Li, X., Matsui, T., Mohr, K., et al. (2014). The Goddard Cumulus Ensemble (GCE) model: Improvements and applications for studying precipitation processes. *Atmospheric Research*, *143*(15), 392–424. https://doi.org/10.1016/j.atmosres.2014.03.005

Tao, W.-K., Lang, S., Zeng, X., Shige, S., & Takayabu, Y. (2010). Relating convective and stratiform rain to latent heating. *Journal of Climate*, *23*(7), 1874–1893. https://doi.org/10.1175/2009JCLI3278.1

Tao, W.-K., & Simpson, J. (1989). Modeling study of a tropical squall-type convective line. *Journal of the Atmospheric Sciences*, *46*(2), 177–202. https://doi.org/10.1175/1520-0469(1989)046<0177:MSOATS>2.0.CO;2

Tao, W.-K., & Simpson, J. (1993). The Goddard Cumulus Ensemble model. Part I: Model description. *Terrestrial, Atmospheric and Oceanic Sciences*, *4*(1), 35–72. https://doi.org/10.3319/TAO.1993.4.1.35(A)

Tao, W.-K., Simpson, J., Baker, D., Braun, S., Choud, M.-D., Ferrier, B., et al. (2003). Microphysics, radiation and surface processes in the Goddard Cumulus Ensemble (GEC) model. *Meteorology and Atmospheric Physics*, *82*(1–4), 97–137. https://doi.org/10.1007/s00703-001-0594-7

Tao, W.-K., Simpson, J., Lang, S., Sui, C.-H., Ferrier, B., & Chou, M.-D. (1996). Mechanisms of cloud-radiation interaction in the tropics and midlatitudes. *Journal of the Atmospheric Sciences*, *53*(18), 2624–2651. https://doi.org/10.1175/1520-0469(1996)053<2624:MOCRII>2.0.CO;2

Tao, W.-K., Simpson, J., & Soong, S.-T. (1987). Statistical properties of a cloud ensemble: A numerical study. *Journal of the Atmospheric Sciences*, *44*(21), 3175–3187. https://doi.org/10.1175/1520-0469(1987)044<3175:SPOACE>2.0.CO;2

Tao, W.-K., Simpson, J., & Soong, S.-T. (1991). Numerical simulation of a subtropical squall line over Taiwan Strait. *Monthly Weather Review*, *119*(11), 2699–2723. https://doi.org/10.1175/1520-0493(1991)119<2699:NSOASS>2.0.CO;2

Tao, W.-K., Simpson, J., Sui, C.-H., Ferrier, B., Lang, S., Scala, J., et al. (1993). Heating, moisture and water budgets of tropical and midlatitude squall lines: Comparisons and sensitivity to longwave radiation. *Journal of the Atmospheric Sciences*, *50*(5), 673–690. https://doi.org/10.1175/1520-0469(1993)050<0673:HMAWBO>2.0.CO;2

Tao, W.-K., & Soong, S.-T. (1986). A study of the response of deep tropical clouds to mesoscale processes: Three-dimensional numerical experiments. *Journal of the Atmospheric Sciences*, *43*(22), 2653–2676. https://doi.org/10.1175/1520-0469(1986)043<2653:ASOTRO>2.0.CO;2

Tao, W.-K., Wu, D., Lang, S., Chern, J.-D., Peters-Lidard, C., Fridlind, A., & Matsui, T. (2016). High-resolution NU-WRF simulations of a deep convective-precipitation system during MC3E: Further improvements and comparisons between Goddard microphysics schemes and observations. *Journal of Geophysical Research: Atmosphere*, *121*(3), 1278–1305. https://doi.org/10.1002/2015JD023986

Wang, D., Giangrande, S. E., Feng, Z., Hardin, J. C., & Prein, A. F. (2020). Updraft and downdraft core size and intensity as revealed by radar wind profilers: MCS observations and idealized model comparisons. *Journal of Geophysical Research: Atmospheres*, *125*(11), e2019JD031774. https://doi.org/10.1029/2019JD031774

Wang, D., Giangrande, S. E., Schiro, K. A., Jensen, M. P., & Houze, R. A., Jr. (2019). The characteristics of tropical and midlatitude mesoscale convective systems as revealed by radar wind profilers. *Journal of Geophysical Research: Atmospheres*, *124*(8), 4601–4619. https://doi.org/10.1029/2018JD030087

Wang, D., Prein, A. F., Giangrande, S. E., Ramos-Valle, A., Ge, M., & Jensen, M. P. (2022). Convective updraft and downdraft characteristics of continental mesoscale convective systems in the model gray zone. *Journal of Geophysical Research: Atmospheres*, *127*, e2022JD036746. https://doi.org/10.1029/2022JD036746

Wang, Y., Tao, W.-K., & Simpson, J. (1996). The impact of ocean surface fluxes on a TOGA COARE convective system. *Monthly Weather Review*, *124*(12), 2753–2763. https://doi.org/10.1175/1520-0493(1996)124⟨2753:TIOOSF⟩2.0.CO;2

Xie, S., Cederwall, R. T., & Zhang, M. (2004). Developing long-term single-column model/cloud system-resolving model forcing data using numerical weather prediction products constrained by surface and top of the atmosphere observations. *Journal of Geophysical Research*, *109*(D1), D001104. https://doi.org/10.1029/2003JD004045

Yanai, M., Esbensen, S., & Chu, J. (1973). Determination of average bulk properties of tropical cloud clusters from large-scale heat and moisture budgets. *Journal of the Atmospheric Sciences*, *30*(4), 611–627. https://doi.org/10.1175/1520-0469(1973)030<0611:DOBPOT>2.0.CO;2

Yoneyama, K., Zhang, C., & Long, C. N. (2013). Tracking pulses of the Madden-Julian Oscillation. *Bulletin of the American Meteorological Society*, *94*(12), 1871–1891. https://doi.org/10.1175/BAMS-D-12-00157.1

Zhang, M. H., & Lin, J. L. (1997). Constrained variational analysis of sounding data bases on column-integrated budgets of mass, heat, moisture, and momentum: Approach and application to ARM measurements. *Journal of the Atmospheric Sciences*, *54*(11), 1503–1524. https://doi.org/10.1175/1520-0469(1997)054<1503:CVAOSD>2.0.CO;2

Zhang, M. H., Lin, J. L., Cederwall, R. T., Yio, J. J., & Xie, S. C. (2001). Objective analysis of ARM IOP data: Method and sensitivity. *Monthly Weather Review*, *129*(2), 295–311. https://doi.org/10.1175/1520-0493(2001)129<0295:OAOAID>2.0.CO;2

Zipser, E. J., & LeMone, M. A. (1980). Cumulus vertical velocity events in GATE. Part II: Synthesis and model core structure. *Journal of the Atmospheric Sciences*, *37*(11), 2458–2469. https://doi.org/10.1175/1520-0469(1980)037<2458:CVVEIG>2.0.CO;2